Multi-omics analysis of paracetamol exposure identifies dysregulated genes involved in neurotoxicity and neuronal differentiation of human embryonic stem cells

Mari Spildrejorde[$,1,2,3], Athina Samara[$,4,5,*], Ankush Sharma[6,7,8], Magnus Leithaug[1,2,#], Martin Falck[1,8,§], Stefania Modafferi[2,+], Arvind Y. M. Sundaram[2], Ganesh Acharya[9,10], Hedvig Nordeng[1,11], Ragnhild Eskeland[1,7,*], Kristina Gervin[**,1,11,12], Robert Lyle[**,1,2,13]

[$] Equal co-authorship contribution
[*] Corresponding author
[**] Equal co-authorship contribution

[1]PharmaTox Strategic Research Initiative, Faculty of Mathematics and Natural Sciences, University of Oslo, Norway
[2]Department of Medical Genetics, Oslo University Hospital and University of Oslo, Norway
[3]Institute of Clinical Medicine, Faculty of Medicine, University of Oslo, Oslo, Norway.
[4]Division of Clinical Paediatrics, Department of Women's and Children's Health, Karolinska Institutet, Sweden
[5]Astrid Lindgren Children's Hospital, Karolinska University Hospital, Stockholm, Sweden
[6]Department of Informatics, University of Oslo, Norway
[7]Department of Molecular Medicine, Institute of Basic Medical Sciences, Faculty of Medicine, University of Oslo, Oslo, Norway
[8]Department of Biosciences, University of Oslo, Norway
[9]Division of Obstetrics and Gynecology, Department of Clinical Science, Intervention and Technology (CLINTEC), Karolinska Institutet, Alfred Nobels Allé 8, SE-14152, Stockholm, Sweden.
[10]Center for Fetal Medicine, Karolinska University Hospital, SE-14186 Stockholm, Sweden.
[11]Pharmacoepidemiology and Drug Safety Research Group, Department of Pharmacy, University of Oslo, Norway
[12]Division of Clinical Neuroscience, Department of Research and Innovation, Oslo University Hospital, Oslo, Norway
[13]Centre for Fertility and Health, Norwegian Institute of Public Health, Oslo, Norway
[#]Current address: Department of Analysis and Diagnostics, Section for Molecular Biology, Norwegian Veterinary Institute, Ås, Norway
[§]Current address: Department of Medical Genetics, Oslo University Hospital and University of Oslo, Norway
[+]Current address: Istituto di Genetica Molecolare, CNR - Consiglio Nazionale delle Ricerche, Pavia, Italy.

Abstract

Background: Several epidemiological studies have found associations between long-term prenatal exposure to paracetamol and neurodevelopmental outcomes in childhood. Pharmacoepigenetic studies have identified differences in DNA methylation (DNAm) in cord blood between exposed and unexposed neonates. However, the causal implications and impact of prenatal long-term paracetamol exposure on brain development are not known.

Methods: We exposed human embryonic stem cells (hESCs) undergoing *in vitro* neuronal differentiation to daily changes of media containing amount of paracetamol corresponding to human foetal exposure with maternal therapeutic doses. An integrated multi-omics approach was used to investigate epigenetic and transcriptomic effects of paracetamol on the early stages of human brain development.

Results: Multi-omics analyses of DNAm, chromatin opening, and gene expression identified dose-dependent effects on cell proliferation and maturation. We found differentially methylated and/or expressed genes involved in signal transduction, neurotransmitter secretion and cell fate determination trajectories. Integration of single-cell RNA-seq and ATAC-seq showed that paracetamol-induced changes in chromatin opening were linked to transcription. For example, *EP300* encoding a histone acetyltransferase and H3K27ac were linked to many putative cis regulatory elements and downregulated upon paracetamol exposure. Some of the genes are involved in neuronal injury, response to toxic insults and development-specific pathways, such as *KCNE3*, overlapped with differentially methylated genes previously identified in cord blood associated with prenatal paracetamol exposure.

Conclusion: We identified dose-dependent epigenetic and transcriptional changes in hESCs undergoing neuronal differentiation after paracetamol exposure. The overlap of differentially methylated genes with our previous analysis in cord blood from children exposed to paracetamol during pregnancy could suggest a causal role in impaired neurodevelopment.

Keywords

paracetamol, acetaminophen, pregnancy, epigenetics, brain development, hESCs, neurotoxicity, scRNA-seq, DNA methylation, scATAC-seq, single-cell, multi-omics

Background

Exposure to medications during pregnancy poses potential teratogenic risks to the developing foetus. More than 80% of women use at least one type of medication during pregnancy (1), and the majority of these medications lack robust safety data. Evaluation of medication safety during pregnancy is difficult due to perceived safety and ethical issues that arise around conducting clinical trials in pregnant women. Moreover, long-term neurodevelopmental consequences of medication exposure during pregnancy have received limited attention. Considering the increasing prevalence and socioeconomic burden of neurodevelopmental disorders (NDDs) (2), identifying risk factors, including medications used during pregnancy is of great importance.

Paracetamol (also known as acetaminophen) is the most widely used analgesic and antipyretic during pregnancy, and it is considered safe for use as the first line option for pregnant women in need of mild analgesics or antipyretics (1,3–5). A number of large epidemiological studies have reported an association between long-term maternal paracetamol use during pregnancy and increased risk of adverse neurodevelopmental outcomes, such as Attention Deficit/Hyperactivity Disorder (ADHD), in the child (6–14). The association is reported to be stronger with long-term exposure and higher dose (15). In 2019, the EUs pharmacovigilance safety committee (PRAC) reviewed all the available evidence from literature, including non-clinical and epidemiological studies, regarding the impact of prenatal paracetamol exposure on impaired neurodevelopment in offspring. In March 2019, PRAC concluded that the available evidence is inconclusive, and recommended that the summary of product characteristics (SmPC) of paracetamol containing products should be updated to reflect the current state of scientific knowledge; "*Epidemiological studies on neurodevelopment in children exposed to paracetamol in utero show inconclusive results*" (PRAC, 2019; 16). More recently, a group of researchers published a consensus statement and literature review in Nature Reviews Endocrinology concluding that there is growing evidence supporting the hypothesis that in utero exposure to paracetamol can impair foetal development (17). This conclusion is still highly debated and contested by others (ENTIS, 2021; 18), reflecting a need for further research.

In a recent study, our group identified an association between DNAm differences in cord blood and long-term paracetamol exposure (> 20 days) during pregnancy in children with an ADHD diagnosis. These findings suggest that DNAm might be involved in the pathogenesis of ADHD (19), but the causality and effect on neuronal differentiation and brain development is not known. It is well established that normal prenatal neurodevelopment involves cellular differentiation and establishment of cell-type specific epigenetic patterns, and that these events are prone to influences by environmental factors. For instance, maternal smoking has been shown to induce DNAm changes and modulate risk of NDDs (20–22). If and how paracetamol modulates the apparent increased risk of NDDs is currently unknown.

Recently, we established a protocol for neuronal differentiation of human embryonic stem cells (hESCs), which can be used in neuropharmacological studies (23). In the present study,

we have used this model system of early human brain development and investigated the effects of paracetamol exposures on transcriptional and epigenetic regulation. Paracetamol doses were selected to reflect therapeutic maternal doses and foetal in utero exposures (24–26). The time and dose effect of paracetamol exposure during differentiation was inferred by integrating multiple omics methods (bulk RNA-seq, bulk DNAm, single-cell RNA-seq and ATAC-seq).

Results

Experimental set-up

We investigated epigenetic and transcriptomic effects of exposure to paracetamol using an *in vitro* neuronal differentiation protocol that drives hESCs towards anterior neuroectoderm (23,27). In brief, the neural induction phase (Stage I) ends at Day 7, the self-patterning phase (Stage II) ends at Day 13, and the FGF2/EGF2-induced maturation phase (Stage III) ends at Day 20 (**Fig. 1A**). Culture media were replaced daily, and the cells were exposed to 100 or 200 μM paracetamol during differentiation from Day 1 and onwards. These concentrations have been documented to be in the range of therapeutic plasma concentrations (24–26). All culture media (control and paracetamol-supplemented) were replaced daily, and unexposed (control) and paracetamol-exposed cells were harvested for downstream analyses on Day 7 and 20. As paracetamol exposure could potentially result in gene expression changes in proliferation or delay differentiation, control cells were also harvested at the onset of differentiation (hESCs; Day 0), and on the intermediate timepoint that cells were passaged (Day 13).

The timeline of brightfield images of the control cells versus cells exposed to 100 (P100) or 200 μM paracetamol (P200) documents the morphological changes and cell culture density at differentiation Days 2, 4, 7, 8, 10, 13, 14, 17 and 20 (**Fig. 1B**). The tightly packed neuroepithelial cells forming the neural rosettes by Day 7 reassembled at the next stage under high density cell passaging and proceeded to maturation. We did not observe any distinct morphological changes in the differentiating cultures exposed to 100 (P100) or 200 μM paracetamol (P200). However, preliminary paracetamol titration experiments showed that exposing the differentiating cells to 400 μM paracetamol increased cell death and unpatterned morphology in cells and were thus discontinued. A set of representative images following the 20-day timeline in control cultures and 100, 200 and 400 μM paracetamol-exposed cells is presented in supplemental information (**Fig. S1**)

Validation of differentiation markers

The protocol efficiency was validated using digital droplet PCR (ddPCR), where the effect of paracetamol on gene expression was assessed at Days 7 and 20 (**Fig.1C**). The ddPCR results showed that the expression of the pluripotency transcription factors (TFs) *POU5F1* and *NANOG* decreased significantly after neural induction. As anticipated, the expression of the neural markers *SOX2*, *OTX2*, *FOXG1* and *MAP2* were increased on Day 7. Increased expression of genes encoding the structural proteins *VIM*, *TUBB3* and TF *NEUROD1* was

more pronounced on Day 13. Notably, the expression of *FOXG1*, *MAP2* and *NES* was significantly different between exposed and control cells on Day 7. Differential expression upon paracetamol exposure was also documented for filament *NES* and TFs *PAX6* and *NEUROD1* on Day 20.

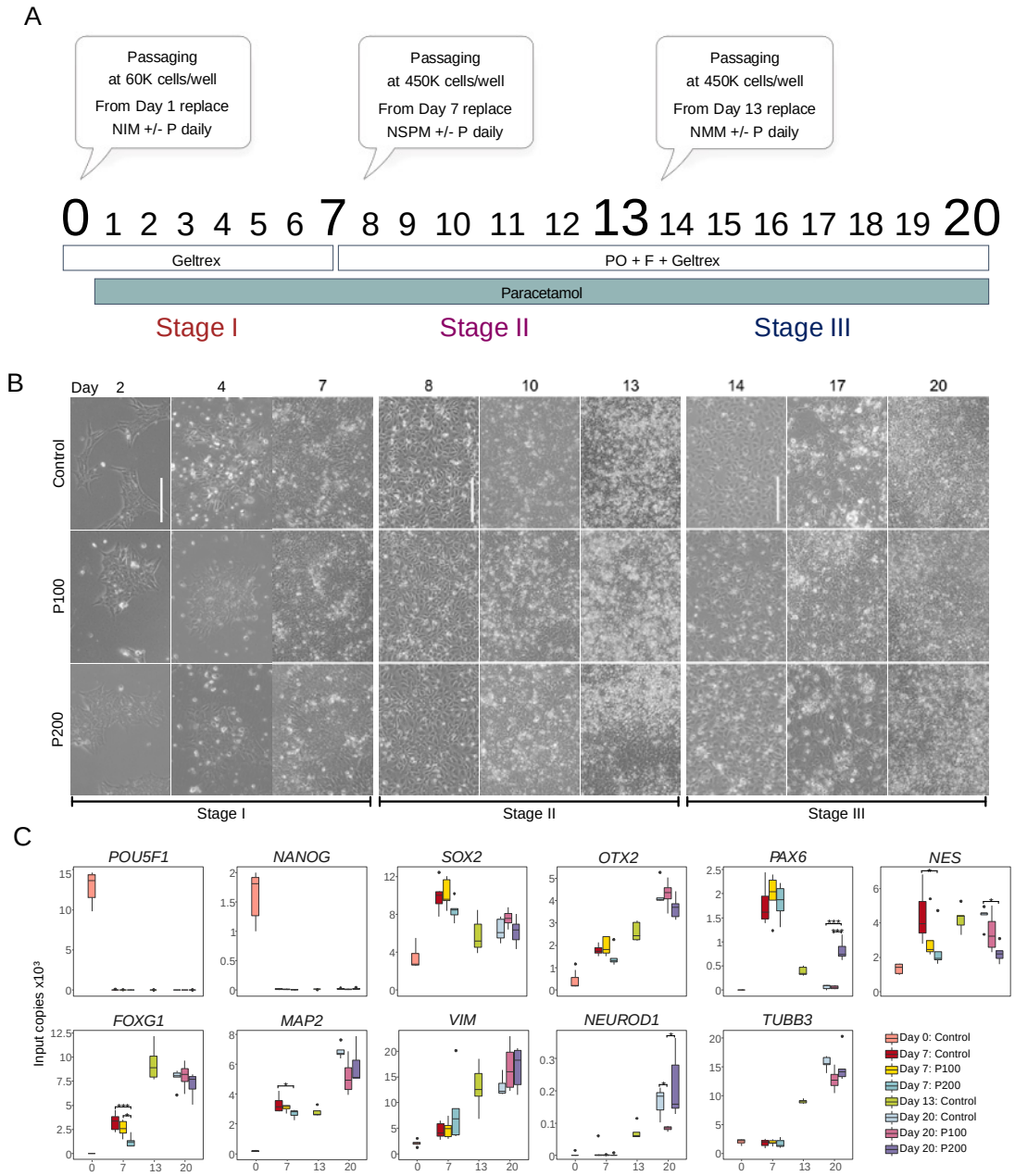

Figure 1. Neuronal differentiation of hESC to model neurodevelopmental effects of paracetamol.
A) Schematic illustration of the different phases of the neuronal differentiation protocol from Day 0 to Day 20. Cells were exposed to 100 or 200 μM paracetamol from Day 1 and onwards. The effect of paracetamol on gene expression and epigenetic profiles was evaluated at Day 7 and Day 20. B) Representative brightfield images of the differentiation timeline for control, P100 or P200 cells during differentiation at Day 2, 4, 7, 8, 10, 13, 14, 17 and 20 (scale bar corresponds to 100 μm). C) ddPCR results from 4-6 replicates of mRNA expression of selected

marker genes from Days 0, 7, 13 and 20. Significant comparisons are marked with asterisks (Student's t-test, *: p <= 0.05, ***: p <= 0.001).

Paracetamol induced changes in DNAm during neuronal differentiation

To assess whether exposure of hESCs undergoing neuronal differentiation to paracetamol induced DNAm changes, we analysed control cells and cells exposed to 100 (P100) and 200 μM paracetamol (P200) at Day 7 and 20. The experimental set-up included analysis of control cells harvested at Day 0 and 13 as reference points of possible dysregulation (**Fig. 2** and **S3, Table S1**). First, we assessed the global effect using principal component analysis that showed clustering of samples according to differentiation day (**Fig. S3A**). Overall, the distribution of DNAm was indistinguishable across exposed and control cells at all time points regardless of paracetamol dose (**Fig. 2A**). In contrast, non-CpG DNAm levels decreased during differentiation and were lower in cells exposed to 200 μM paracetamol compared to control cells at Day 20 (**Fig. 2B**).

To investigate whether the cells exposed to different doses of paracetamol (P100 and P200) respond differently than control cells from Day 7 to Day 20, we performed a DNAm time-response analysis. We observed no significant DNAm changes in P100 compared to control between Day 7 and Day 20 (not shown). In contrast, 3113 CpGs responded differently to P200 compared to control cells over time (**Fig. 2C**). CpGs showing an increase in DNAm are annotated to genes with key functions in dynamic cellular redox changes in the developing brain, such as the neural specification gene *PRDM16* (28). CpGs showing a decrease in DNAm are annotated to genes enriched for gene ontology (GO) terms involved in synaptic regulation, GABAergic signalling and cell morphogenesis (**Fig. 2D**). CpGs showing an increase in DNAm are annotated to genes enriched for GO terms such as synaptic signalling and chemical synaptic transmission (**Fig. 2D**). Overall, when we assessed DNAm levels at all CpGs (**Fig. 2E**) compared to all significant CpGs (**Fig. 2F**), we found a general dose-dependent increase in DNAm levels at significant sites in paracetamol-exposed cells compared to controls at both Day 7 and Day 20. The annotation of differentially methylated CpGs (DMCs) in relation to genes and CpG islands was similar across the different comparisons (**Fig. S3B-C**).

Next, we performed comparisons of DNAm levels in paracetamol-exposed cells to controls at Day 7 (**Fig. S3D-F**, **Table S1**) and Day 20 (**Fig. S3E-G**, **Table S1**) for the different doses. As expected, there were more significant DNAm changes after longer exposure (Day 20) and at higher concentration of paracetamol (P200) (**Table S1**). At Day 7, there were no dose dependent DMCs whereas at Day 20 a larger number of CpGs (n=8940) were differentially methylated between P100 and P200. Moreover, there was some overlap between DMCs at 7 and Day 20 (**Fig. S3H**).

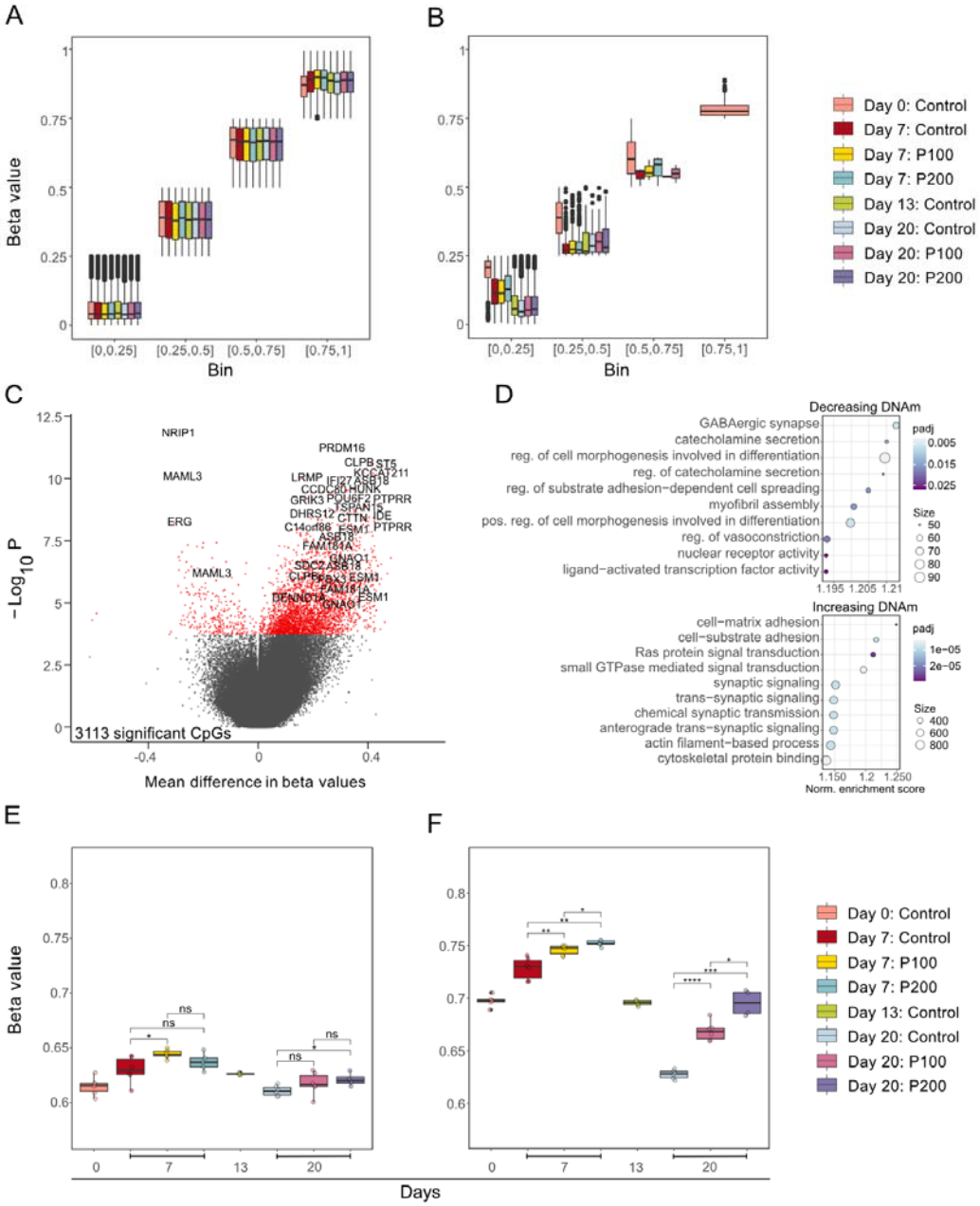

Figure 2. Exposure to paracetamol induces changes in DNAm over time during neuronal differentiation. A) Average DNAm levels for each sample across all CpGs and non-CpGs (grouped in bins of 0.25) at different days in controls and cells exposed to different paracetamol doses. B) Average DNAm levels for each sample across all non-CpGs (grouped in bins of 0.25) for all controls and exposed cells. C) Volcano plot showing the effect of 200 μM paracetamol from Day 7 to Day 20. CpGs with adjusted p-value < 0.05 were considered significant. D) Corresponding enriched GO-terms for CpGs showing a decrease in DNAm (top) or an increase in DNAm (bottom) over time (Day 20 – Day 7) in P200 cells compared to control cells. E) Average DNAm levels per sample for all CpGs across differentiation for Day 0, 7, 13, and 20. F) Average DNAm levels per sample for all significant CpGs (paracetamol-exposed cells vs control comparisons) at Day 0, 7, 13, and 20. E-F) *p < 0.05, **p < 0.01, ***p < 0.001, ****p < 0.0001.

Paracetamol-induced gene expression changes in genes involved in neural development

To delineate the effect on gene expression, we performed bulk gene expression analysis using RNA-seq in controls and paracetamol exposed cells (P100 and P200; **Fig. 3**, **S4** and **Table S1**). Principal component analysis showed that samples clustered according to differentiation day (**Fig. S4A**). Overall, when we compared P100 and control we identified 121 differentially expressed genes (DEGs, **Fig. 3A**) and 1433 DEGs between P200 and control (**Fig. 3B**) from Day 7 to Day 20 (**Table S1**). Pairwise comparisons between paracetamol (P100 and P200) and control at each day are shown in **Fig. S4B-C**. We also confirmed that the bulk RNA-seq analysis of the previously selected marker genes (**Fig. 1B**) correlates well with the ddPCR results of selected marker genes (**Fig. S2**).

Gene set enrichment analyses (GSEA) identified enrichment of GO terms and biological processes (BPs) in P100 and P200 cells from Day 7 to Day 20 compared to controls. These analyses identified enrichment of downregulated BPs involved in synaptic organization, transmission and regulation in the P100 time-response analysis (**Fig. 3C**). Notably, the upregulated BPs in the P200 time-response analysis were enriched for forebrain regionalization, cerebellar cortex formation and hindbrain differentiation (**Fig. 3D**). Also, the DEGs associated with P100 and P200 were enriched for common BPs reflecting enrichment of transmitter transport and regulation, synaptogenesis, synaptic organization and plasticity.

The bulk RNA-seq pairwise comparisons of the P100 and P200 paracetamol-exposed cells to controls, showed an overlap of several DEGs (**Fig. S4D-F**). Exposure to paracetamol was associated with downregulation of genes previously linked to migration and neural development (e.g. *NTRK3*, *PMEL* (29), *CCDC184* (30), *MYT1* (31,32). Furthermore, we identified DEGs linked to synaptic organization and transduction (e.g. *MYO16* (33), *HS3ST4* (34), *SORCS3* (35)), metabolism (*GCK* (36)), neuronal survival, dendrite branching, axonal growth and neural projection in development (e.g. *NSG1* (37), *TMEM3C6* (38), *TMOD1* (39), *PLPPR4* (40), *NEBL* (41), *NRN1*(42) and *GFRA2* (43)) and channelopathies (e.g. *CACNA1B/C* (44), *SCN3A* (45)) (**Fig. 3E**). Thus, these bulk RNA-seq analyses revealed transcriptional dysregulation of genes related to possible developmental delays between control and paracetamol-exposed cells.

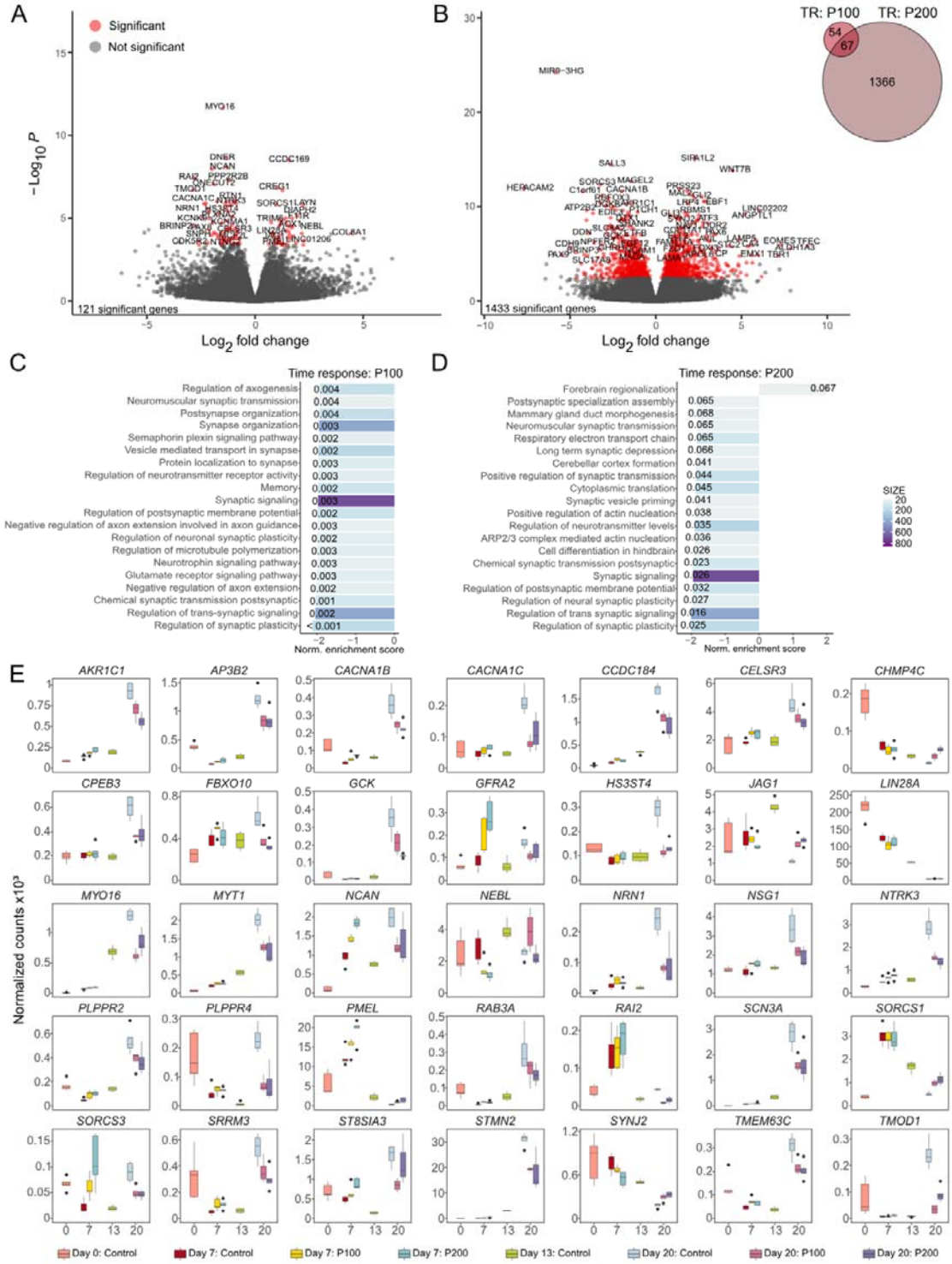

Figure 3. Paracetamol exposure of differentiating hESCs modulates expression of genes involved in neural development. Volcano plots of longitudinal differences in gene expression in A) P100 and B) P200 cells from Day 7 to Day 20. Corresponding Venn diagram shows the number of overlapping DEGs between the time-response (TR) of the two concentrations of paracetamol. Top 20 enriched BPs in C) P100 cells and D) P200 cells over time. E) Gene expression levels of selected DEGs, which overlapped between TR P100 and TR P200.

To define a regulatory role of paracetamol induced DNAm changes on gene expression, we assessed the overlap between DEGs and DMGs for the pairwise comparisons and time response analyses (**Table S1**). The percentage of DMGs overlapping with DEGs varied between 3 and 63 % for the different comparisons. The P200 time response analysis revealed 180 overlapping genes, and some selected genes are visualized in **Figure 4**. DNAm levels for *GRIK3*, *CACNA1D*, *ABAT*, *MAPT* and *ANKRD6* were inversely correlated with gene expression, whereas DNAm levels for *PAX7*, *CDH2* and *WNT7B* were positively correlated with gene expression at Day 20. *GLI3* is an example of a gene where DNAm levels are correlated with both negative and positive regulation (**Fig. 4**).

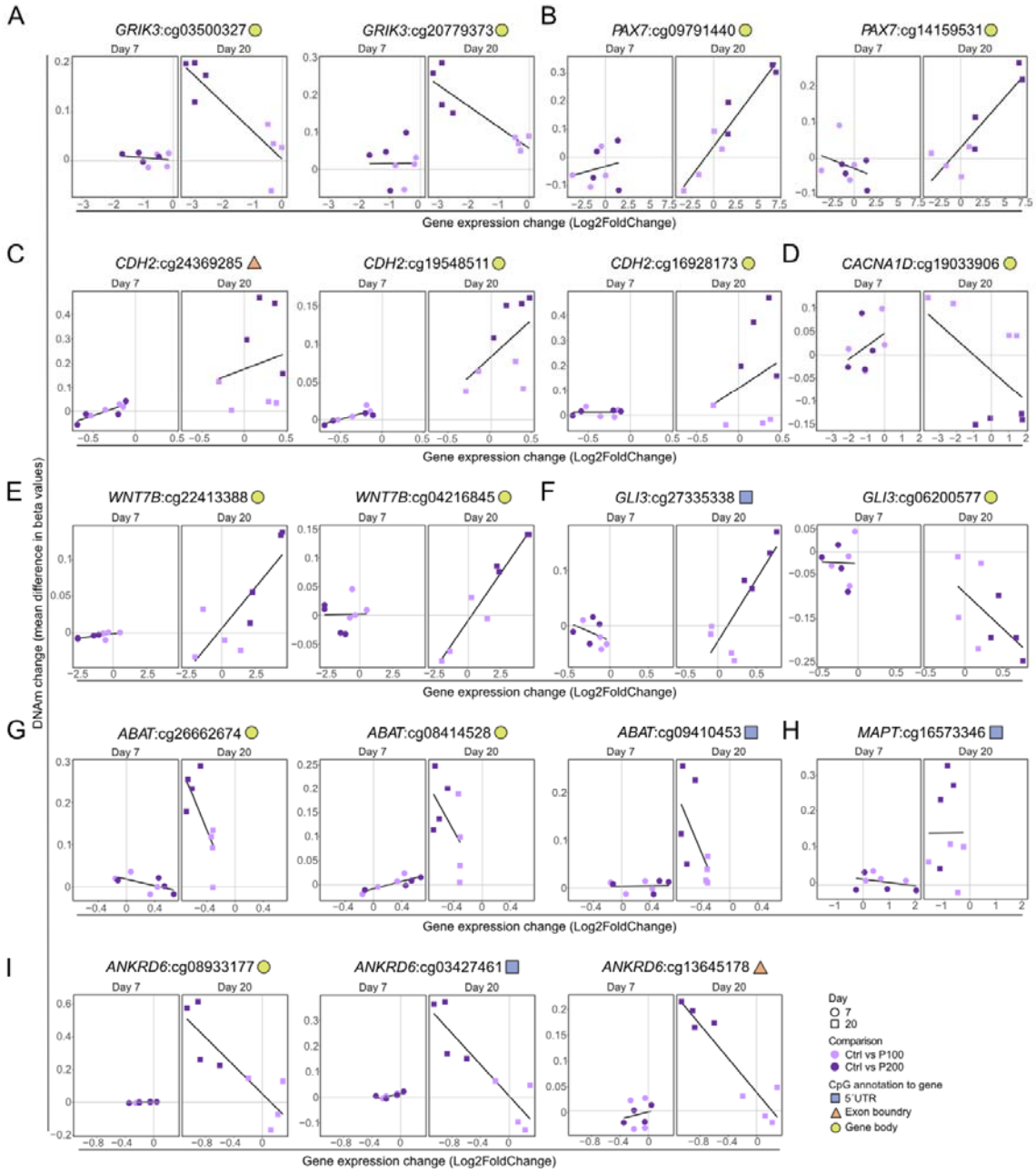

Figure 4. DNAm and gene expression for selected overlapping DMCs and DEGs. Change in DNAm and gene expression levels between control and P100 or P200 for A) *GRIK3*, B) *PAX7*, C) *CDH2*, D) *CACNA1D*, E) *WNT7B*, F) *GLI3*, G) *ABAT*, H) *MAPT* and I) *ANKRD6*. Each point represents a matched replicate between RNA-seq and DNAm and black lines represents a linear regression line of the mean of values.

Single-cell RNA sequencing reveals dose-specific changes in several major cellular processes after paracetamol exposure

To explore cell-type specific gene expression and maturation signatures over time, we performed single-cell RNA sequencing (scRNA-seq) analysis of control and paracetamol-exposed cells (P100 and P200) at Days 7 and 20 (**Table S2**). The principal aim was to identify possible deviations and alternate pathway trajectories or delays in neuronal differentiation compared to the control cells as a result of paracetamol exposure. A total of 15 201 cells (n=6 924 Day 7 cells, n=8 277 Day 20 cells) from two time-course experiments were aggregated and projected in Uniform Manifold Approximation and Projections (UMAPs, **Fig. 5**). The scRNA-seq data may also be visualized in the open access webtool (**hescneuroparacet**), where expression of genes can be explored per cell, cluster and time point. This webtool allows the users to explore the data presented in this study irrespective of their competence in computational biology.

As expected, the cells clustered according to differentiation day and not exposure to paracetamol (**Fig. 5A**). Seurat-predicted cell cycle phase showed an increase in G1 cells at Day 20 (**Fig. 5B**), which is consistent with previous results (27). However, the existing cell cycle analysis tools are unable to decipher the proportion of neurons that are in G0 phase. Also as expected, the CytoTRACE pseudotime differentiation trajectory analysis showed that cells were most differentiated at Day 20 (**Fig. 5C**). Empirically defined Seurat clusters are shown at resolution 0.4 with the corresponding single-gene annotations of the cell types resolved in the composite neuronal differentiation datasets (**Fig. 5D**). The P1-P13 clusters were annotated by the genes *CRABP1*, *PAX6*, *TYMS*, *KIF20A*, *FGF17*, *HES5*, *WNT5A*, *ASCL1*, *GNG8*, *DLX1*, *SRSF9*, *VEPH1* and *TAGLN2*, respectively. At Day 7, there was a subtle shift in cell composition from P1 to P2 in the cells exposed to paracetamol (**Fig. 5E)**. The effect was more prominent at Day 20 with a higher proportion of paracetamol-exposed cells compared to controls annotated to cluster P5 and a more prominent effect at P200 exposure, whereas a lower proportion were annotated to P6, P9 and P10 for both concentrations (**Fig. 5E**).

For preliminary cell identity annotation, the data were juxtaposed with a scRNA-seq Human Brain dataset (46). Most cells at Day 7 were similar to neuronal progenitors, whereas cells at Day 20 were similar to neuronal progenitors, neuroblasts and neurons (**Fig**. **5F**). At Day 20, there was a subtle shift from cells annotated to neuroblasts towards the less differentiated neuronal progenitors in paracetamol-exposed cells compared to controls (**Fig**. **5G).** UMAP plots of the dual co-expression of the genes *ID2/ID4*, *CDK1/CDKN1C*, *HES1/STMN2*, *REST/NEUROD1*, *NKX2.1/WNT7B* and *NTRK.1/DLX6-AS1* indicate agreement between these maturation signatures and the CytoTRACE trajectory analysis (**Fig. 5C** and **H**).

The analysis of the top DEGs per cluster (**Fig. S5**) and a thorough data exploration (**Fig. S6)**, showed that paracetamol exposure induced changes in several major processes at the selected timepoints. In brief, at Day 7 we identified dose-dependent changes that link paracetamol exposure to cell-cycle transition important in neuronal maturation, as shown by the expression of known proliferation-related genes such as *MKI67, PCNA, TP53, CDK1, MYBL2* and *GJA1* (**Fig. S6)**. We further documented expression changes of genes known to be involved from the onset of neural induction towards and throughout differentiation, or its inhibition (*REST, RAX, PAX6, HES1, HES5, ID3* and *ID4),* neurite outgrowth and cortical neurogenesis (*GBA2, ASPM*), neuronal maturation *(CDKN1C, POU2F1, POU3F1, ROBO1, STMN2* and *STMN4)* and WNT and FGF signalling (*FRZB, WNT4, WNT7B, FGF8* and *FGFRL1)* (**Fig. S6)**. Differential and dose dependent expression of crucial spatiotemporally regulated transcription factors associated with brain development (e.g., *NKX2.1, OTX2, FOXG1, ASCL1, ISL1, EMX2* and *HOXA1*), neurotransmitter transporter expression (*SAT1*, *SLC2A1*) was also assessed and identified. Finally, we found differential expression of genes related to cellular response to toxic insults (e.g., *DDR1)* (**Fig. S6)**.

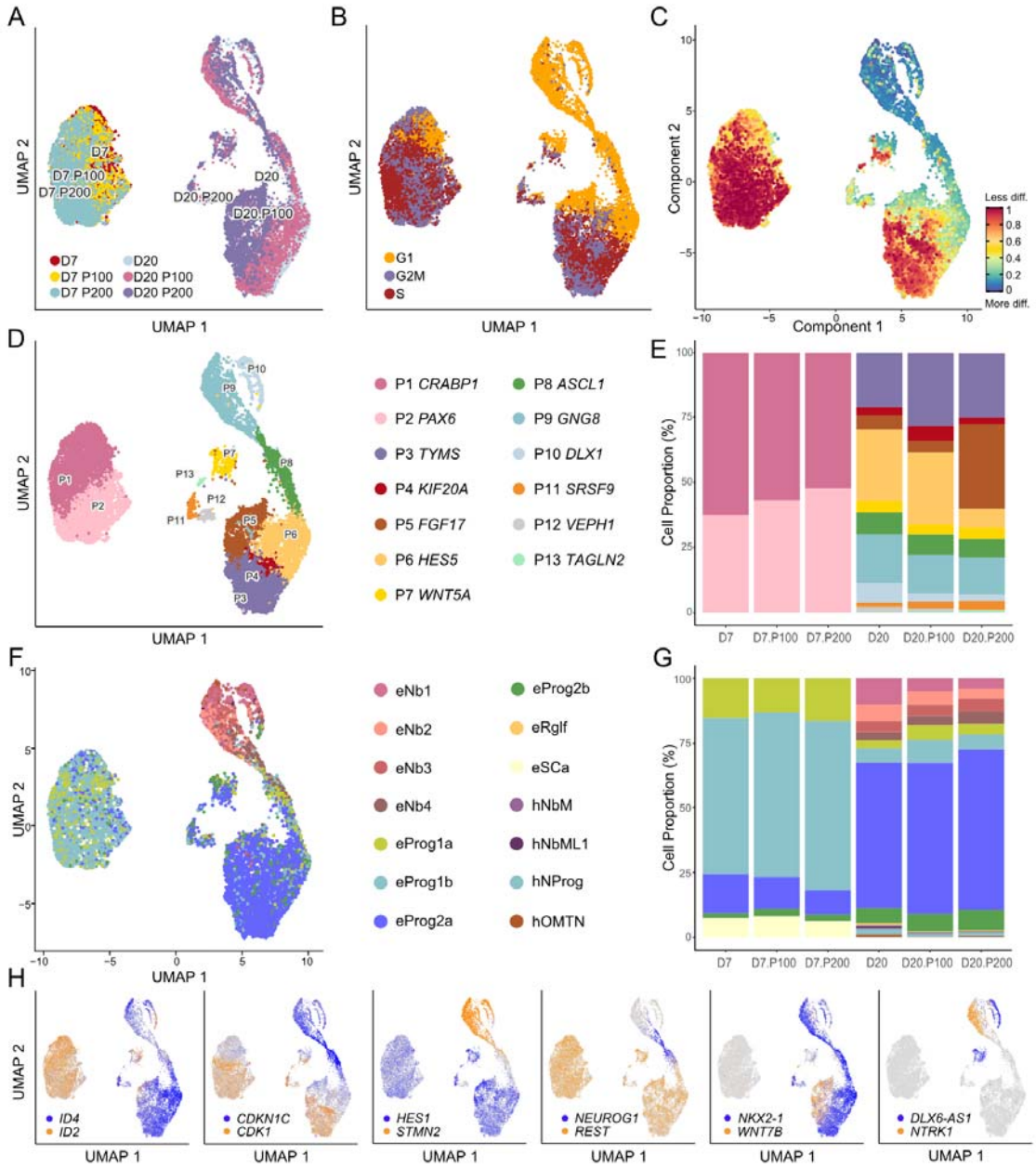

Figure 5. scRNA-seq analysis revealed shifts in cell type composition of differentiating cells exposed to paracetamol. Day 7 and Day 20 control cells and cells exposed to 100 μM (P100) or 200 μM (P200) paracetamol were visualized with UMAP and coloured by A) sample identity, B) Seurat predicted cell cycle phase, C) CytoTRACE pseudotime differentiation trajectory, D) defined Seurat clusters at resolution 0.4 with corresponding gene annotations and E) cell proportions per cluster. F) UMAP plots of cells coloured by SingleR cell annotation to Human Brain reference with corresponding cell annotations. Cell types starting with "e" are hESC derived cells and cell types starting with "h" are *in vivo* human embryo cell types. Nb1-4; neuroblasts, Prog1-2; neuronal progenitors, Rglf; radial glia-like cells, SCa; stem cells, NbM; medial neuroblasts, NbML1; mediolateral neuroblasts, NProg; neuronal progenitors, OMTN; oculomotor and trochlear nucleus. G) Corresponding cell proportions per cell type. H) UMAP plots of dual gene coexpression for *ID2/ID4*, *CDK1/CDKN1C*, *HES1/STMN2*, *REST/NEUROD1*, *NKX2.1/WNT7B* and *NTRK.1/DLX6-AS1* indicate that maturation signatures agree with the CytoTRACE trajectory analysis.

Paracetamol exposure is associated with differential expression of neural lineage markers

To extract the biological significance and interpretation of DEGs after paracetamol exposure in the scRNA-seq datasets, we performed GO analyses and identified enrichment of GO terms and BPs. First, we identified the top 10 upregulated and downregulated BPs between control cells and P100 (**Fig. 6A**) or P200 cells (**Fig. 6B**) on Day 7. Notably, BPs involved in *DNA replication* and *cell-cycle regulation* were upregulated in cells exposed to both paracetamol doses, and a downregulation of a BP which involves *generation of neurons*. DEGs in P100 cells compared to control cells were enriched for more neuronal specific annotations. Furthermore, P200 compared to control cells identified upregulated GO terms involved in cellular responses to toxic insults and *DNA checkpoint activation*. The top 20 DEGs between P100 (**Fig. 6C**) or P200 (**Fig. 6D**) and control cells at Day 7, are shown as bubble plots of relative gene expression. The gene expression of the top overlapping genes between the P100 and P200 cells compared to control cells at Day 7 (**Fig. 6E**) extends the GO annotations to gene specific similarities. We identified changes in crucial genes, such as the master gene of forebrain development *FOXG1* (47) and genes of the *HES* and *ID* gene families involved in differentiation and neurogenesis (48).

Next, we extracted the top 10 upregulated and downregulated BPs among the DEGs between control cells and P100 (**Fig. 6F**) or P200 cells (**Fig. 6G**) on Day 20. In both comparisons, downregulated GO terms included *neuron/nervous system developmen*t and *microtubule polymerization or depolymerization*. Of the top 20 DEGs at Day 20 between paracetamol-exposed and control cells, we found major patterning TFs, such as *NKX2.1* and *EMX2* (**Fig. 6H-I)**. Moreover, genes that belong to the ZIC family, among other genes involved in Notch and Wnt signalling, were also identified (**Fig. 6H-I)**. The gene expression of the top overlapping genes between P100 and P200 cells were compared to control cells at Day 20 (**Fig. 6J**). The analysis of GO terms delineated gene specific changes, such as upregulation of *SELENOW* (**Fig. 6D**), previously associated with neuroprotection from oxidative stress (49). The paracetamol-induced differentiation lag as evidenced by the *PAX6* expression in the P200 cells (**Fig. 1C**). Downregulation of tissue- and stage- specific genes, such as *FABP7*, *ISL1*, *STMN2* and *INA* were also identified. In addition, *TUBB1A*, the isotype associated with postmitotic neurons (50), and *TUBB2B*, that constitutes 30% of all brain beta tubulins (51), were also found among the downregulated genes. Interestingly, *PEG10* and *C1orf61* (the microRNA9-1 host gene, *MIR9-1HG*) stand out in the Day 20 P200 comparisons. These genes have recently been linked to cortical migration and intercellular communication (52), further documenting how the P200 dose of paracetamol could affect proper network formation and cell to cell signalling.

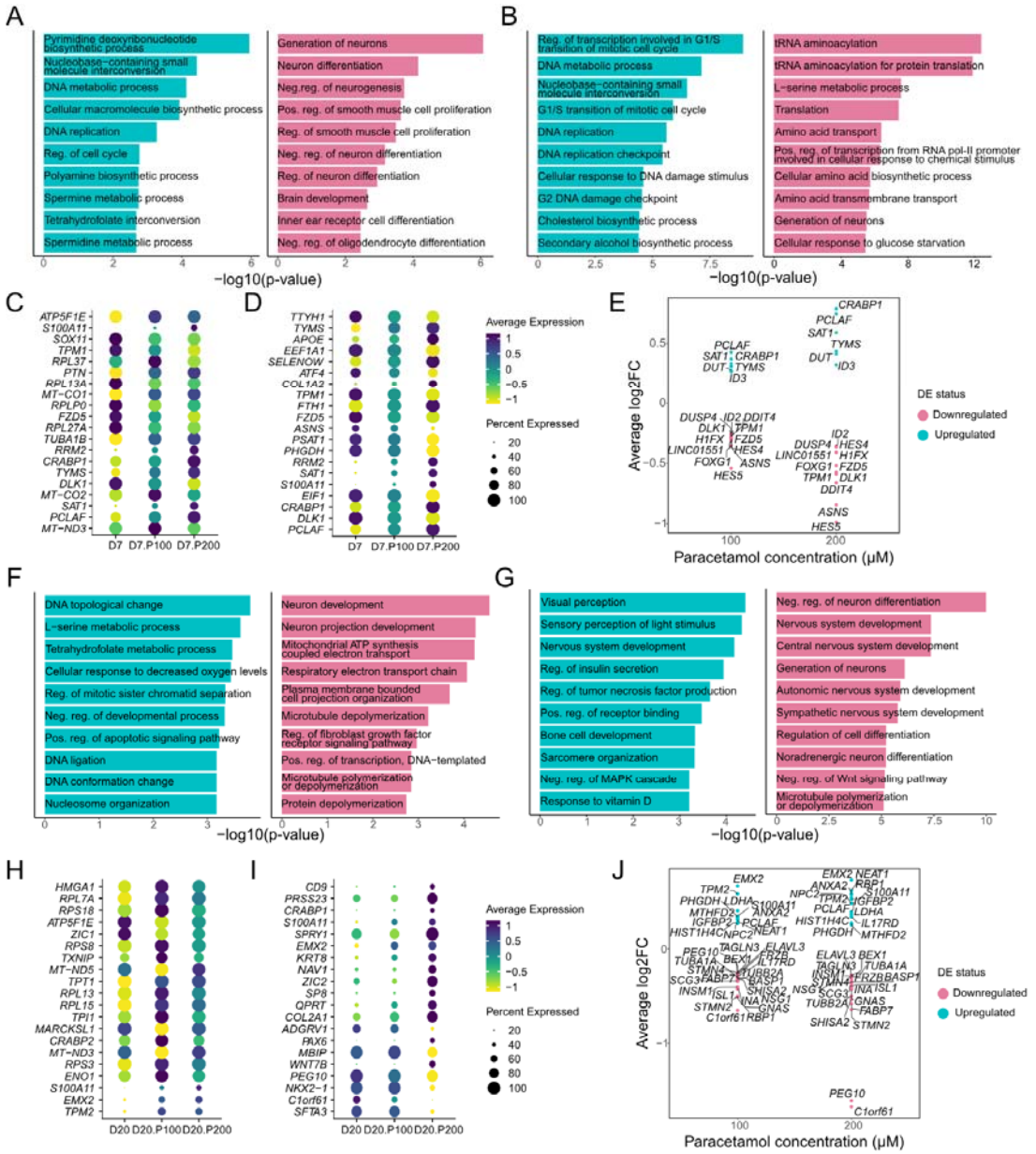

Figure 6. Differential gene expression analysis in single cells showed downregulation of genes involved in neuronal differentiation after paracetamol exposure. A-B) Top 10 upregulated (green) and downregulated (pink) BPs among DEGs at Day 7 between A) P100 or B) P200 and control cells. C-D) Bubble plot showing gene expression for the top 20 DEGs at Day 7 between C) P100 or D) P200 and control cells. E) Gene expression of top overlapping genes between P100 and P200 cells compared to control cells at Day 7. F-G) Top 10 upregulated (green) and downregulated (pink) BPs of DEGs at Day 20 between F) P100 or G) P200 and control cells. H-I) Bubble plot showing gene expression for the top 20 DEGs at Day 20 between H) P100 or I) P200 and control cells. J) Gene expression of top overlapping genes between P100 and P200 cells compared to control cells at Day 20.

Integration of scATAC- and scRNA-seq link paracetamol-induced changes in chromatin opening to transcriptional activity at Day 20

We used scATAC-seq to understand whether paracetamol exposure during differentiation influenced the chromatin landscapes at Day 20. We obtained 3 042 nuclei for Day 20 control and 3 480 and 4 282 nuclei for Day 20 exposed to 100 µM (P100) and 200 µM paracetamol (P200), respectively. First, we reanalysed scRNA-seq data from Day 20 controls, P100 and P200, and remapped the P3-P13 clusters (**Fig. 7A-B**). The maturation trajectory cohered with the initial Day 7-Day 20 time point analysis (**Fig. 7C and 5C**). Next, we mapped the scATAC-seq data (**Fig. 7D**) to 15 scATAC-seq clusters (C1-C15; **Fig. S7A**) that we integrated with the annotated scRNA-seq P3, P5, P9, P10 and P13 clusters (**Fig. 7E)**. The quality of the combined scATAC-seq datasets was documented with an even distribution of integrated clusters (P3, P5, P9 and P10) over TSS, promoters, exons, introns and distal genomic regions (**Fig. S7B-C**). The P13 cluster represented a very low number of nuclei and displayed lower enrichment across all genomic regions.

To further explore the differential chromatin accessibility across the genome, we correlated distal accessible regions with gene expression (53). This allows for identification of putative cis regulatory elements (CREs) for biological and functional comparisons of Day 20 control cells with P100 and P200 exposed cells. We grouped the peak-to-gene links (P2GLs) into five clusters and plotted heatmaps of gene expression and gene scores for all three datasets (P2GLs represent potential genes linked to chromatin opening, **Fig. 7G-I**). We observed relatively similar numbers of putative CREs in controls (n=30 771), P100 (n=26 216) and P200 (n=28 883). Notably, the heatmaps of controls and P100 and P200 cells were different with an absence or presence of the integrated cluster P5, also described as having differential prominence in the scRNA-seq data (**Fig. 5E**). Only 6960 of the putative CREs overlapped between the three datasets, whereas 4 732, 3 435 and 6 534 putative CREs specifically overlapped between control and P100, control and P200, and P100 and P200, respectively (**Fig. 7J** and **Table S3A-C**). Moreover, we observed that many of the putative CREs were only detected in individual datasets (Day 20 control; n=15 644, P100; n=10 460 and P200; n=12 304 CREs). These variations in putative CREs suggests that paracetamol exposure induced changes in chromatin accessibility. For example, in the locus of the neuronal marker gene *STMN2,* which showed higher gene expression in unexposed cells compared to exposed cells, also showed changes in chromatin opening peaks in paracetamol exposed cells (**Fig. S7D, 6J** and **S6**). Furthermore, accessibility peaks in the *ELAVL4* locus displayed differential chromatin opening in clusters P3, P5, P9 and P10. We also identified putative CREs in the exposed cells that correlated with higher *ELAVL4* expression in control cells compared to P100 or P200 cells (**Fig. 7K** and **Table S3A-C)**.

Paracetamol affects region-specific chromatin accessibility

The putative enhancer-gene interactions identified likely represent chromatin regulomes in the control and the paracetamol-exposed cells. We therefore compared the level of overlap of linked genes to better understand the effect of paracetamol exposure on chromatin regulation. A larger proportion of linked genes overlapped between the Day 20 control and paracetamol exposed cells (n=4 047), and the P100 (n=1 224) and P200 (n=1 048) cells (**Fig. 7L** and **Table S3A-C** and **V**). GO analyses of the linked genes revealed a common enrichment of

BPs, such as *nervous system development*, *biological regulation*, *neurogenesis*, and *neuron differentiation*, varying in the different K-means (km) clusters (**Fig. S7D** and **Table S3D-F**). Linked genes identified in paracetamol exposed cells (P100; n = 652, P200; n = 915 and 1424 for both P100 and P200) indicate exposure-induced changes in gene. Interestingly, linked genes including neuronal lineage transcription factors (e.g. *PAX6*, *NEUROD4*, *NEUROG1*, *SOX9* and *SOX2*) and genes involved in chromatin modification (e.g. histone H3K27 acetyltransferase *EP300* (54), Histone H3K27me3 demethylase *KDM6A* (55) and chromatin remodeller SNF2 subfamily member *SMARCAD1* (56)), suggest that paracetamol may contribute to modulation of transcriptional regulation and chromatin structure (**Table S3V**). In addition, GO analysis of the putative CREs identified enrichment of BPs per k-means group and sample are shown in **Tables S3G-U**.

Further, we identified enriched TF motifs in the CREs that may infer gene expression program regulation. Specifically, several identified TFs (n=29) that were common for control, P100 and P200 cells, including *NEUROD1*, *NEUROG1*, *SOX9*, *HMGA1* and several members of the ONECUT and NHLH families, which have previously been described in the neuronal differentiation protocol (27). These analyses identified TFs that were common in P100 and P200 cells (n=18) or dependent on paracetamol dose (**Fig. 7L-M, 6I, S6, S7F** and **Table S4**). The TF footprint per cluster and motif enrichment and computed sequence logos for *OTX2*, *TBR1* and *EMX2* show that these factors are enriched and potentially regulate genes in these integrated clusters (**Fig. 7O)**. In particular, *OTX2* motifs were enriched in cluster 5 that mostly represents cells from P100 and P200 exposure.

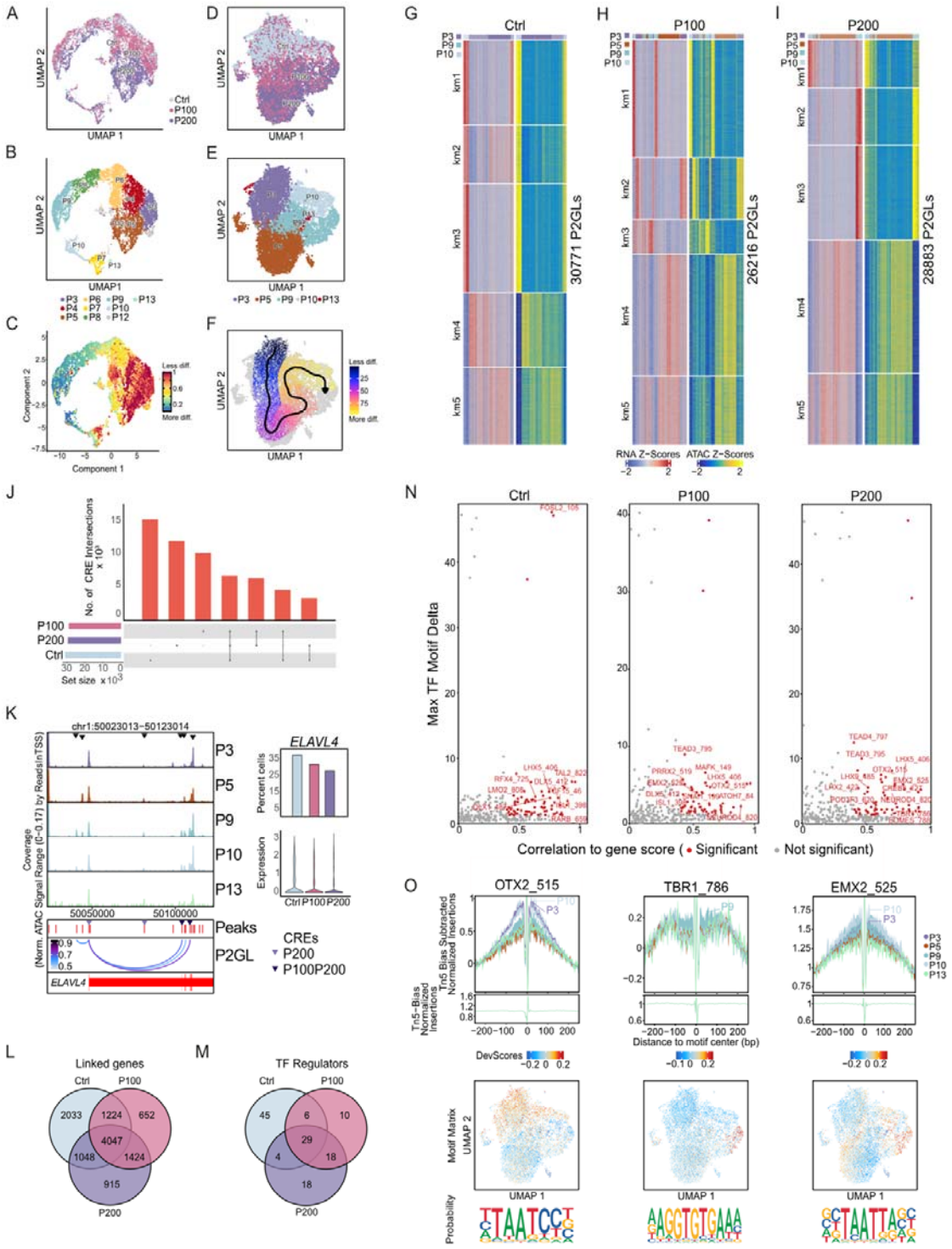

Figure 7. Effects of paracetamol on chromatin accessibility and integration with scRNA-seq at Day 20. A-C) scRNA-seq UMAP plots coloured by A) sample identity, B) scRNA-seq clusters or C) CytoTRACE pseudotime differentiation trajectory. D-E) scATAC-seq UMAP plots of coloured by D) sample identity and E) remapped clusters following constrained alignment of cell populations by scATAC-seq and scRNA-seq integration. F) Supervised pseudotime trajectory of integrated clusters. G-I) Heatmaps of scATAC-seq and scRNA-seq side-by-side representing peak to gene links (P2GLs) in G) control cells, H) P100 cells and I) P200

cells. Rows were clustered using k-means (k = 5). J) Overlap of putative CREs from P2GLs analyses of Day 20 control versus P100 and P200. K) *ELAVL4* locus browser view (GRCh38.p13) from 5000 cells with ATAC-seq signals in integrated clusters. Differential chromatin opening (black triangles), ATAC peaks (red), P2GLs (arcs) and putative CREs enriched in P200 or P100 and P200 cells (coloured triangles) are shown. The bar plot to the right shows the corresponding percentage of cells expressing *ELAVL4*, and the plot below represent the expression levels. L) A Venn diagram representing overlap of linked genes. M) Venn diagram of TF regulators identified from P2GL integrative analysis. N) A selection of positive TF regulators computed using gene integration scores with motifs in the putative CREs. O) Footprints for selected TF regulators OTX2, TBR1 and EMX2 demonstrating preferential opening per cluster; below are the corresponding ArchR motif deviation scores, motif matrix and representative sequence logos identified in the scATAC-seq dataset.

Overlap of dysregulated genes in differentiating hESCs and cord blood from children exposed to paracetamol during pregnancy

We have previously identified an association between differential DNAm in cord blood and long-term paracetamol exposure during pregnancy in children with ADHD (19). To assess the translational potential and causality of these findings, we compared the dysregulated genes identified in the present model to the differentially methylated genes associated with paracetamol exposure in cord blood. In brief, the DMCs and the DEGs in paracetamol-exposed differentiating cells at Day 20 were compared to DMGs in cord blood (19). Interestingly, the results from these analyses identified an overlap between DEGs and DMCs for P100 and P200 in differentiating hESCs and differentially methylated genes identified in cord blood between paracetamol-exposed children with ADHD versus controls (**Fig. 8A**) and paracetamol-exposed children with ADHD versus ADHD controls (**Fig. 8B**). There were 20 differentially methylated and expressed genes in the first comparison (i.e., paracetamol exposed cells vs. paracetamol-exposed children with ADHD versus controls) and only one gene (*KCNE3*) in the second comparison (i.e., paracetamol-exposed cells vs. paracetamol-exposed children with ADHD versus ADHD controls). Specifically, the overlapping genes were *BMP4, CD82, CHFR, CRISPLD2, DPF3, ELFN2, GAB2, GPR153, GPR160, HCN1, IER3, KCNE3, MYCBPAP, NOTCH4, PDGFRA, PTCH2, SGK1, SLC22A23, SPRED2* and *ZDHHC14.*

The gene expression of the 20 overlapping genes is presented both in bubble plots using our webtool (scRNA-seq data **Fig. 8C**) and in box plots (bulk RNA-seq data **Fig. 8D**). Notably, genes involved in differentiation, such as *GAB2* (57), or *Notch and Hedgehog signalling pathways* (such as *NOTCH4* (58), *PTCH2* (59) *SHISA2* (60)) show a dose-dependent downregulation of expression in paracetamol-exposed cells compared to controls. This high variation in expression levels after paracetamol exposure compared to controls, indicates a dose effect. Among genes identified at Day 7 in the P200 cells, we observed upregulation of genes such as *ZDHHC14* (61) and *SGK1* (62), previously associated with control of neuronal excitability and neuronal response to injury, respectively. Several toxic insult response genes were also upregulated at Day 20 in the P200 cells, such as *IER3* (63), *SPRED2* (64), *GPR130* (65), and *SLC22A23* (66).

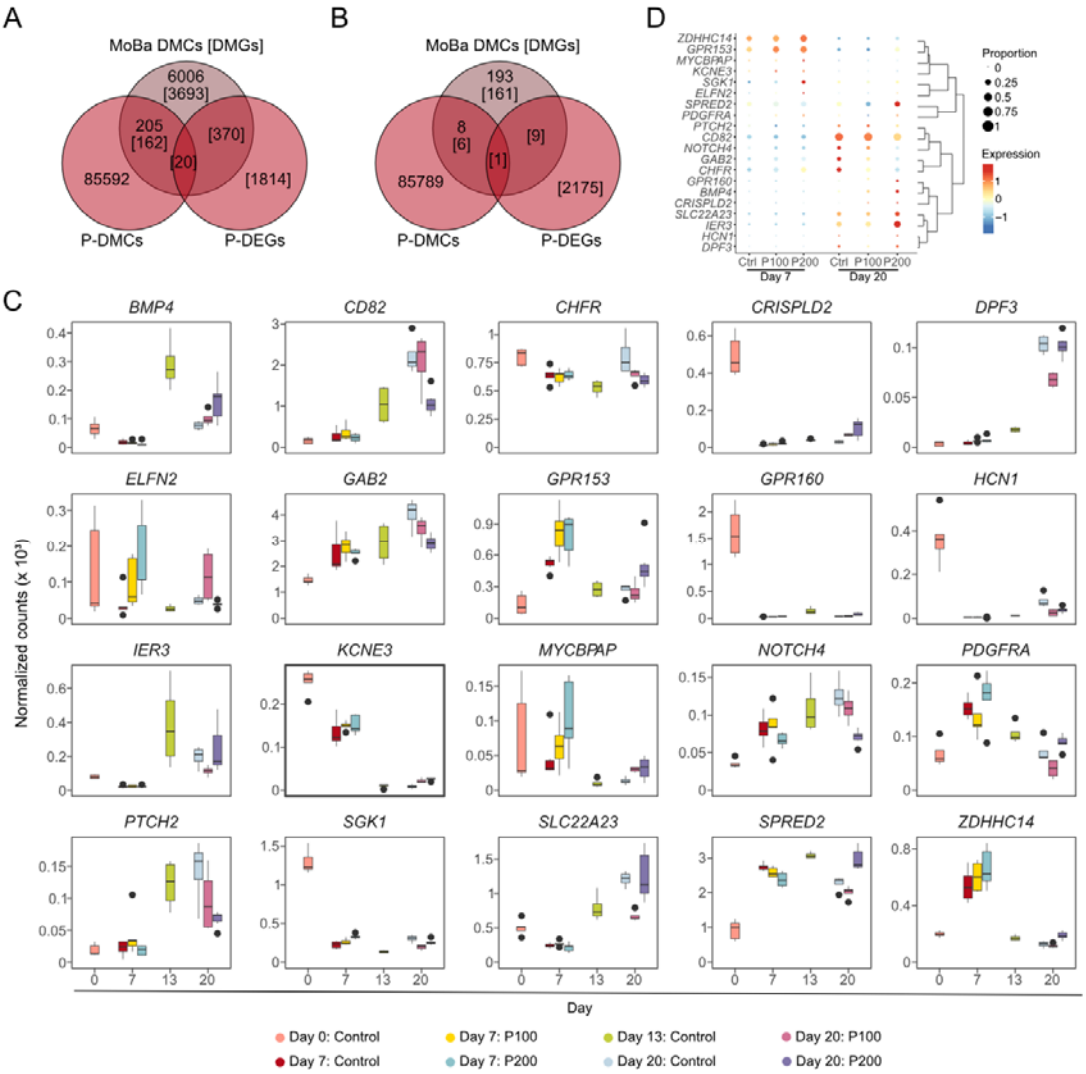

Figure 8. Overlap with differentially methylated genes in cord blood. A-B) Venn diagrams showing the overlap between DEGs and DMCs for P100 and P200 and A) paracetamol-exposed children with ADHD versus controls and B) paracetamol-exposed children with ADHD versus ADHD controls in cord blood. C-D) Gene expression levels of overlapping genes identified in cord blood derived from C) RNA-seq and D) scRNA-seq data.

Discussion

To our knowledge, this is the first multi-omics study investigating how paracetamol exposure affects epigenetic and transcriptional programmes involved in early brain development using an *in vitro* hESC model of neuronal differentiation (27).

Analyses of DNAm in differentiating cells exposed to different doses of paracetamol identified a general dose-dependent increase in DNAm in exposed cells compared to controls at both Day 7 and Day 20. These genes were enriched for BPs involved in cell morphogenesis and adhesion, but also synaptic transmission and signalling with a focus on catecholamines and GABAergic transmission. Considering that this is an *in vitro* system, the findings are compelling since structural cortical changes and catecholaminergic transmission have been the target of various epidemiological studies and drug clinical trials, both in children and adults with ADHD (67–70).

We performed both bulk and scRNA-seq, and the analyses identified differential expression of genes enriched for BPs involved in transmitter transport and regulation, synaptic organization and synaptogenesis and plasticity. Interestingly, in cells exposed to the high dose of paracetamol (P200), we also identified enrichment of GO categories reflecting possible patterning deviations from forebrain differentiation. Thus, we observe an effect of paracetamol exposure on transcriptional dysregulation and possible developmental delays during neuronal differentiation. Additionally, among the common DEGs, irrespective of paracetamol dose, we identified *SORCS3,* which encodes a brain-expressed transmembrane receptor associated with neuronal development and plasticity that has been previously identified in a GWAS meta-analysis of ADHD significant risk loci (71).

The scRNA-seq analysis enabled investigation of gene expression in individual cells and identified dose-dependent DEGs involved in several major processes during neuronal differentiation. Exposure to paracetamol resulted in a subtle shift in cell populations from P1 to P2 at Day 7. At Day 20 the P6, P9 and P10 clusters decreased whereas P5 markedly increased in P200. The DEGs link paracetamol exposure to genes involved in cell-cycle length and phase transition and genes important for neuronal maturation, neurite outgrowth, cortical neurogenesis, expression of neurotransmitter transporters, neuronal maturation and WNT and FGF signalling. Further, the data also documented dose-dependent differential expression of crucial spatiotemporally regulated TFs associated with brain development. These findings provide evidence of transcriptomic dose-dependent effects of paracetamol exposure related to cellular response to toxic insults and fate-determination deviation queues at the Day 20. Furthermore, the results identified an impact of paracetamol exposure on the regulation of central, autonomic and sympathetic nervous system development, which are all central to fine-tuning human cognition and associated with ADHD (72–74).

To further characterize and investigate epigenetic mechanisms involved in altered cellular heterogeneity and differentiation, we performed scATAC-seq to map CREs and compare the chromatin landscape changes between control and cells exposed to P100 and P200 at Day 20

(**hescneurodiffparacet**). Interestingly, the results from these analyses identified differences in several chromatin accessible regions in genes previously associated to fate mapping and neurogenesis, which have been identified in risk determination studies focusing on cognition and autism spectrum disorders (e.g. *DLK1, DIO3, IPW* (75,76)) and ADHD (e.g. *MEG3* (77)). Genome-wide association studies (GWAS) suggest that cognitive disorders might also result from the cumulative effect of gene variant regulation and parent-of-origin effect (77), which in ADHD has been associated with genes such as *DDC, MAOA, PDLIM1* and *TTR*. We also identified chromatin openness differences related to genes identified in the paracetamol exposed cells. For example, *PCDH7*, which acts as a positive cue for axonal guidance via roles in cell adhesion, was among the genes that were both differentially expressed and had different chromatin openness in Day 20 P200 cells. Dysregulation of *PCDH7* could be relevant to the semaphorin-plexin signalling documented by the enriched BPs in the P100 cells, and it is noteworthy as it has also been associated to ADHD (71). We also identified dose-dependent differences in chromatin accessibility of the neural specification gene locus *PRDM16*, which correlates well with DNAm analyses where exposure to paracetamol was associated with increased DNAm at CpGs annotated to *PRDM16*. This gene has been linked to regulation of transcriptional enhancers activating genes involved in intermediate progenitor cell production and repressing genes involved in cell migration (28). The molecular mechanism of *PRDM16* remains unknown, but has been associated with reactive oxygen species regulation in the embryonic cortex (78).

Integrative analyses of scRNA-seq and scATAC-seq to explore the links between chromatin accessibility and gene expression documented high correlation and showed an overlap between scATAC-seq modalities and scRNA-seq cell clusters. This analysis identified novel putative CREs, and linked genes affected by paracetamol exposure. Although a portion of linked genes overlapped between the control and exposed cells, there was only a small overlap between the putative CREs. This suggest that many local changes in chromatin opening were affected by paracetamol exposure and that these CREs regulate the different gene expression programmes in control and paracetamol exposed cells. How paracetamol regulates chromatin opening is not known, and we have limited knowledge on the effect of paracetamol on the TFs recognition of DNA motifs. However, our data suggest that genes linked to putative CREs that were affected by paracetamol exposure have a role in regulation of transcription and chromatin. In particular, a linked gene specific for paracetamol exposure was *EP300*, which is encoding a histone acetyltransferase responsible for the active enhancer mark H3K27ac (79). *EP300* expression decreased subtly upon paracetamol exposure both at Day 7 and 20, and these changes in EP300 levels may therefore change the number of active enhancers in the paracetamol exposed cells. Furthermore, we identified TFs such as EMX2, TBR1 and OTX2 whose regulatory activity is affected by paracetamol exposure at the differentiation end point. This is suggestive of a mechanism for how paracetamol exposure may change gene expression programmes in early brain development. More work is needed to follow up the functional role of paracetamol exposure on the enhancer regulation and gene expression.

It is biologically plausible that medications that cross the placenta and the blood-brain barrier, may interfere with normal foetal brain neurodevelopment, previously shown for valproic acid, and more recently for topiramate (80). This is especially relevant for substances that cross the blood-brain barrier, which is considered functional by the 8th week of gestation (81). However, invasive testing of the foetal compartment in human is rarely indicated, which makes data on safety during pregnancy for most substances scant. Thus, most pharmacoepigenetic studies address associations of DNAm differences in cord blood or placenta from neonates delivered at term exposed to the maternal medication during pregnancy, which is also the case for paracetamol (82–84). We have previously published a study of cord blood samples from the Norwegian Mother, Father and Child cohort (MoBa), where we found differentially methylated genes in cord blood from children with ADHD exposed to long-term maternal paracetamol use (19). However, the causality, and relevance of such findings to brain development are not known. Thus, we aimed to investigate the effect of long-term paracetamol exposure at therapeutic doses during the early stages of human brain development. The hESCs used in our experiments represent the inner cell mass (ICM) of Day 6 -preimplantation- blastocysts (85). The ICM is known to differentiate to form the primitive ectoderm around Day 7.5 post fertilization (86), but placental circulation is not established before Day 17-20 (87). Prior to this, the fraction of paracetamol that reaches the developing embryo does so via passive diffusion (88). Interestingly, irrespective of the temporal differences of the two models, comparing the differentially expressed and methylated genes identified in our study revealed overlap of several genes identified in cord blood with potential compelling relevance to early brain development. Notably, identification of a dose-specific effect on several genes have previously been shown to be associated with neural injury and toxic-insult response (89–91). To our knowledge this is the first study that has identified an effect of paracetamol on differential DNAm of *KCNE3* in a neuronal differentiation model of hESCs. Differential DNAm at *KCNE3* was also identified in our MoBa study in cord blood. Furthermore, *KCNE3* was also identified in a DNAm analysis of extremely low gestational age new born (ELGAN) cohort (84). *KCNE3* is an interesting candidate, which encodes a voltage-gated ion channel with important functions in regulating release of neurotransmitters and neuronal excitability (92,93). Among the overlapping genes, there was also *IER3*, whose differential DNA methylation at specific CpG sites has been previously associated with *in utero* exposure to bisphenol A (BPA) (94). The same study had identified *TSPAN15*, which is also significantly differentially methylated between control and P200 cells in our neuronal differentiation model.

We also compared our data to previously published studies using the webtool (**hescneuroparacet**). In a rat model of foetal paracetamol exposure (95), dysregulation in specific ABC efflux transporters and related enzymes was found after chronic treatment of the mothers in E19 foetal brain and choroid plexus. In our model of paracetamol exposure, we also identified differential expression of the relevant genes *ABCA1, ABCC5, ABCD3* and *GSTM*3. Moreover, the expression of *ABCC4*, which encodes the multidrug resistance-associated protein MPRP4, known to play a role in paracetamol efflux was also upregulated at Day 20 (96). In another model assessing chronic paracetamol exposure effects in E15-19 rat brains (97), similar to our findings, an increased expression of genes related to proliferation

(e.g. *MKI67*, *MTDH*), cytoskeletal structural genes (e.g. *NEFL* at Day 20), metabolic stress alleviation (e.g. *PFKP* at Day 7) or decrease in genes related to differentiation (*SOX12* at Day 7) migration and dendrite orientation (such as *CRMP1* at Day 20) was found. Notably, a significant increase in *APOE* expression at P200 cells at Day 7 was observed indicating stress or neuronal damage (98), and a similar response by the increased expression for glutamate transporter *EAAT4* (99). The significant *IL6ST* (GP130) and *MEF2A* (100) upregulation and the similarities of our findings to the other *in vivo* models, validate both the trajectories identified by our approach, and the chosen paracetamol neurotoxicity platform for early development studies.

Our study has several limitations and strengths. Protein expression changes were not explored, as this was beyond the scope of this study. This study aimed to delineate the epigenetic impact of paracetamol on early human cortical developmental events. We used both bulk- and scRNA- seq and comparing these two datasets identified a varying degree of overlapping DEGs from 1-27 %, confirming that both datasets are complementary to detect transcriptomic changes induced by paracetamol. Using a multi-omics approach, we unveiled the diversified transcriptional networks related to paracetamol exposure. We could not accurately classify the maturation properties of the cells, or the quotient of cells in G0 phase, highlighting the necessity of new tools to deconvolute the neuronal G0 phase. The results of scATAC-seq analysis presented here are inherently limited by the relatively low genome-per-cell coverage. That means that some open chromatin regions that could have proved relevant for the individual cells or cell populations, may have been missed. Finally, the *in vitro* results presented here needs to be validated by *in vivo* models and targeted human dataset exploration in future studies. This could confirm whether the pathways identified can explain the paracetamol-induced adverse effects in the early human brain.

Abiding by the Findability, Accessibility, Interoperability, and Reusability (FAIR) principles, we further provide full access to the scRNA-seq and scATAC-seq datasets. These datasets can be visualized in the open access shiny web platforms for scRNA-seq (**hescneuroparacet**) and integrative scATAC-seq/scRNA-seq (**hescneurodiffparacet**) (101,102). Moreover, these webtools also allow for data correlation with other published gene expression datasets, and enable plotting, exporting and downloading high resolution figures of one's genes of interest as gene expression and gene co-expression analysis UMAPs of any gene. Furthermore, there are multiple options for dataset exploration and visualization, such as heatmaps, violin-, box-, proportion- and bubble plots in different tabs, where gene expression may be viewed per cell, cluster, treatment and timepoint. Chromatin opening can be explored for genomic loci of interest for input sample, ATAC clusters or integrated clusters in a genome browser view with peak-to-gene link annotations (instantly plotted for 500 random cells each time). In addition to enabling users to explore the datasets using the web tools, the processed datasets and code are made available for customization and integration with other studies. To our knowledge this is the first *in vitro* study of paracetamol exposure of hESCs under neuronal differentiation, that provides access to scRNA-seq and scATAC-seq data via interactive webtool.

Conclusions

Using an *in vitro* hESC model of neuronal development, we identified altered DNAm, chromatin openness and expression of genes involved in key neuronal differentiation processes at bulk and single-cell levels. An overlap of genes identified in this model and in the cord blood of neonates exposed long-term to paracetamol during pregnancy, points towards altered epigenetic regulation of early brain development. Identification of common DNAm modification sites and chromatin openness regions with a regulatory role on gene expression can identify loci and underlying mechanisms involved in teratogenicity of drugs on the developing foetus with potential effect on long-term neurodevelopmental outcomes. Such findings could strengthen causal inference and clinical translation of altered DNAm, such as in cord blood, on brain development. However, these *in vitro* results need further validation for potential clinical translation.

Methods

hESC culture and maintenance

hESCs HS360 (Karolinska Institutet, Sweden, RRID:CVCL C202) (85,103) were cultured as described by Samara et al, 2022 (23). In brief, cells were maintained in Essential 8™ Medium, on Geltrex pre-coated culture plates. Cells were routinely passaged at 75-85% confluency using 0.5 mM ethylenediaminetetraacetic acid (EDTA) in ratios between 1:3 to 1:6. When hESCs were collected for initiation of the differentiation protocol, Accutase was used to detach and dissociate cells instead of EDTA.

Neuronal differentiation of hESCs and exposure to paracetamol

hESCs HS360 were differentiated, as described by Samara et al, 2022 (23), in two separate time-course experiments, to investigate the *in vitro* effects of paracetamol exposure in physiologically concentrations relevant to long-term exposure *in vivo*. Since paracetamol crosses the placenta and the blood-brain barrier and has an insignificant plasma protein binding, maternal plasma/serum and cord blood concentrations can be used as estimates for the amount of paracetamol that reaches the developing foetal brain (104–107). Concentrations of 100 μM and 200 μM paracetamol (Merck; A7085) were chosen as range for physiological plasma peak concentration *in vivo*, corresponding to one intermediate and one high peak plasma concentration (24–26). Thus, cells undergoing neuronal differentiation were exposed to media changes of medium only (control) or medium containing 100 or 200 μM paracetamol from Day 1 to Day 20. Control cells were harvested at day 0, 7, 13 and 20, while cells exposed to 100 or 200 μM paracetamol were harvested at day 7 and 20 (**Table 1**).

Table 1. Overview of presented datasets.

Day	Control	P100	P200
0	bRNA, m		
7	bRNA, m, scRNA	bRNA, m, scRNA	bRNA, m, scRNA
13	bRNA, m		
20	bRNA, m, scRNA, scATAC	bRNA, m, scRNA, scATAC	bRNA, m, scRNA, scATAC

bRNA; bulk RNA-sequencing, m; DNAm, scRNA; single-cell RNA sequencing, scATAC; scATAC-sequencing.

DNA/RNA isolation

Genomic DNA and total RNA were isolated by direct lysis in the culture vessels followed by column-based isolation using RNA/DNA purification kit (Norgen Biotek). RNase-Free DNase I Kit (Norgen Biotek) was applied for on-column removal of genomic DNA contamination from RNA isolates. Five RNA isolates were processed using the RNeasy Mini

Kit (Qiagen) followed by DNase-treatment using the RNAse-Free DNase Set (Qiagen). All isolations were performed according to the manufacturer's instructions. Nucleic acid quantification was performed using Qubit (ThermoFisher Scientific), purity was measured using Nanodrop 2000 (ThermoFisher Scientific), while RNA and DNA integrity was assessed using 2100 Bioanalyzer (Agilent Technologies) and 4200 TapeStation (Agilent Technologies), respectively.

ddPCR and RNA expression analysis

Reverse transcription of total RNA was performed using QuantiTect Reverse Transcription Kit (Qiagen). Subsequent ddPCR reactions were set up using ddPCR Supermix for Probes (No dUTP) (BioRad) and Taqman assays (ThermoFisher) or Universal Probes (Roche) in combination with target primers (Eurofins) as outlined in **Table 2.** Droplets for ddPCR amplification were generated using the QX200 Droplet Generator (BioRad). Data acquisition and primary analysis was done using the QX200 Droplet Reader (BioRad) and QuantaSoft software (BioRad). All steps were performed according to the manufacturer's instructions. To calculate the number of target copies per ng RNA input, samples were normalized using RPL30 and RAF1 as normalization genes (108). Statistical comparisons were performed in R using t-test in ggpubr package v.0.4.0 (109). Results were visualized in R using the tidyverse package (110).

Table 2. Assays used for ddPCR

TaqMan Assays	
Gene	Cat #
POU5F1	Hs00999632_g1
SOX2	Hs01053049_s1
NANOG	Hs04399610_g1
NES	Hs04187831_g1
FOXG1	Hs01850784_s1
TUBB3	Hs00801390_s1
MAP2	Hs00258900_m1
PAX6	Hs00240871_m1
OTX2	Hs00222238_m1
VIM	Hs00958111_m1
NEUROD1	Hs01922995_s1
RPL30	Hs00265497_m1

Roche Assay	
Gene	Primer sequence
RAF1	F: tgggaaatagaagccagtgaa
	R: cctttaggatctttactgcaacatc
	Probe 56 Universal Probe library

Bulk RNA-seq

The sequencing library was prepared with TruSeq Stranded mRNA Library Prep (Illumina) according to manufacturer's instructions. The libraries (n=39) were pooled at equimolar concentrations and sequenced on an Illumina NovaSeq 6000 S1 flow cell (Illumina) with 100 bp paired end reads. The quality of sequencing reads was assessed using BBMap v.34.56 (111) and adapter sequences and low-quality reads were removed. The sequencing reads were then mapped to the GRCh38.p5 index (release 83) using HISAT2 v.2.1.0 (112). Mapped paired end reads were counted to protein coding genes using featureCounts v.1.4.6-p1 (113). Differential expression analysis was conducted in R version 3.5.1 (114) using SARTools v.1.6.8 (115) and the DESeq2 v.1.22.1 (116), and genes were considered significantly differentially expressed with an FDR < 0.05. Normalized counts were visualized using the tidyverse package v.1.3. (110). The heatmaps were generated using the pheatmap package version 1.0.12 (117). The Wald-test was used to calculate p-values and Benjamini-Hochberg was used to correct for multiple testing. The GSEA analysis of ranked lists of differentially expressed genes were performed using GSEA software v.4.1.0 (118) to identify enrichment of BP terms.

Bulk DNAm analysis

DNAm status of 43 samples were assessed using the Infinium MethylationEPIC BeadChip v.1.0_B3 (Illumina). Quality control and pre-processing of the raw data was performed in R using Minfi v.1.36.0 (119). No samples were removed due to poor quality (detection p values >0.05). Background correction was performed using NOOB method (120) and β values (ratio of methylated signal divided by the sum of the methylated and unmethylated signal) were normalized using functional normalization (121). Probes with unreliable measurements (detection p values >0.01) (n = 12,538) and cross-reactive probes (45) (n = 42,844) were then removed, resulting in a final dataset consisting of 810,477 probes and 43 samples. Probes were annotated with Illumina Human Methylation EPIC annotation 1.0 B5 (hg38). Differential DNAm analysis was performed on the M values (log2 of the β values) using the limma package (122), and CpGs were considered significantly differentially methylated with an FDR < 0.05. GO analysis of BP terms was performed using p-values of increasing or decreasing CpGs (DMCs) as input to methylRRA function implemented in the methylGSA package version 1.14.0. (123).

Collection of cells and scRNA-seq

Cells were washed twice in wells with 1x PBS and detached using Accutase (STEMCELL Technologies) at 37 °C for 7 min. Cells were triturated 10-15 times to separate into single cells and transferred to centrifuge tubes containing the appropriate base media with 0.05 % BSA (Sigma-Aldrich). Counts were performed using Countess II FL Cell Counter (ThermoFisher Scientific) before cells were centrifuged at 300x g for 5 min and the supernatant was discarded. Cell pellets were then resuspended in base medium containing 0.05 % BSA and cell aggregates were filtered out using MACS SmartStrainers (Miltenyi). The cells were recounted and processed within 1 hour on the 10x Chromium controller (10x Genomics). Approximately 2,300 cells were loaded per channel on the Chromium Chip B (10x Genomics) to give an estimated recovery of 1,400 cells. The Chromium Single Cell 3´ Library & Gel Bead Kit v3 (10x Genomics) and Chromium i7 Multiplex Kit (10x Genomics)

were used to generate scRNA-seq libraries, according to the manufacturer's instructions. Libraries from 16 samples were pooled together based on molarity and sequenced on a NextSeq 550 (Illumina) with 28 cycles for read 1, 8 cycles for the I7 index and 91 cycles for read 2. For the second sequencing run, libraries were pooled again based on the number of recovered cells to give a similar number of reads per cell for each sample (33,000 - 44,000 reads/cell).

scRNA-seq data analysis

Pre-processing: The Cell Ranger 3.1.0 Gene Expression pipeline (10x Genomics) was used to demultiplex the raw base-call files and convert them into FASTQ files. The FASTQ files were aligned to the GRCh38 human reference genome, and the Cell Ranger Count command quantified single-cell read counts using default parameters for Days 7 and 20. Cell ranger aggregate was used for aggregating counts of replicates.

Filtering and normalization: The Seurat Package v.4.1.0 (124) was used to perform quality control and normalization on the count matrices. We filtered cells with number of RNA counts >= 2000 & <= 50000 to remove dead cells, doublets and multiplets. The cells expressing fewer genes (less than 200) and genes expressed in less than 3 cells were excluded from the downstream analysis. Outlier cells with high Mitochondrial percentage was computed using Scater package 1.0.4 “isoutlier” function with nmads parameter of 5 (125). Counts were adjusted for cell-specific sampling using the SCTransform function with regression of Cell cycle genes and Mitochondrial content (126,127).

Clustering and Dimensionality reduction: We used a resolution of 0.4 to cluster cells, obtained by determining the optimum number of clusters (cells grouped together sharing similar expression profiles) in the dataset using the Clustree R package (128). Principal component analysis was performed using the RunPCA function, followed by FindClusters and RunUMAP functions of Seurat package to perform SNN-based UMAP clustering.

Differential expression and annotation: FindMarkers from the Seurat R package was used to perform differential expression analysis between groups. For DE between exposure groups, thresholds were set to the following: min.pct = 0.25, min.diff.pct = -Inf, logfc.threshold = 0.1. For top overlapping DE genes per Day (Fig. 6 E/J), thresholds were set to the following: min.pct = 0.25, min.diff.pct = -Inf, logfc.threshold = 0.25. Genes with an adjusted p-value < 0.05 were considered significant. GO analysis was performed using the DEenrichRPlot function of the mixscape R package with the "GO_Biological_Process_2018 " database with the following thresholds: logfc.threshold = 0.25, max genes = 500. The SingleR R package (129) was used to annotate the cells against reference data sets from a Human Brain dataset (46) from the scRNAseq R package (130). Cell types with < 15 cells annotated were excluded from the plots.

scATAC-seq Library preparation and sequencing

Cells were washed twice with 1xPBS and detached to single cell suspension by application of Accutase (STEMCELL Technologies) at 37 °C for 7 min. The detached cells were washed

with appropriate base media with added 0.04% BSA (Sigma-Aldrich) and filtered using MACS SmartStrainers (Miltenyi Biotech) to remove cell aggregates. Nuclei isolation was done according to the 10x Genomics protocol CG000169 (Rev D) using 2 minutes of incubation in a lysis buffer diluted to 0.1x and 0.5x for Day 0 and Day 20 cells, respectively. Countess II FL Cell Counter (ThermoFisher Scientific) was used to quantify nuclei and confirm complete lysis and microscopy to confirm high nuclei quality. Nuclei were further processed on the 10x Chromium controller (10x Genomics) using Next GEM Chip H Single Cell Kit (10x Genomics), Next GEM Single Cell ATAC Library & Gel Bead Kit v1.1 (10 x Genomics) and Chromium i7 Multiplex Kit N Set A (10x Genomics) according to the Next GEM Single Cell ATAC Reagent Kits v1.1 User Guide (CG000209, Rev C). The targeted nuclei recovery was 5,000 nuclei per sample. The resulting 4 sample libraries were sequenced on a NovaSeq Sp flow cell (Illumina) with 50 cycles for read 1, 8 cycles for the i7 index read, 16 cycles for the i5 index read and 49 cycles for read 2.

scATAC sequencing analysis

Cell Ranger ATAC version 1.2.0 with reference genome GRCh38-1.2.0 was used to pre-process scATAC-seq raw sequencing data into FASTQ files. Single-cell accessibility counts for the cells were generated from reads using the *cellranger-atac count* pipeline. Reference genome HG38 used for alignment and generation of single-cell accessibility counts was obtained from the 10x Genomics (https://support.10xgenomics.com/single-cell-atac/software/downloads/). Downstream analysis of the scATAC-seq data was performed using the R package ArchR v1.0.1 (53). A tile matrix of 500-bp bins was constructed after quality control, removal of low-quality cells and doublet removal using the doubletfinder function of ArchR. The ArchR Project contained the filtered cells that had a TSS enrichment below 3 and <1000 fragments. A layered dimensionality reduction approach utilizing Latent Semantic Indexing (LSI) and Singular Value Decomposition (SVD) applied on Genome-wide tile matrix. Uniform Manifold approximation and projection (UMAP) was performed to visualize data in 2D space. Louvain Clustering methods implemented in R package Seurat (124) were used for clustering of the single-cell accessibility profiles.

Availability of data and materials

The single-cell RNA-seq/ATAC-seq, RNA-seq and DNA-methylation data reported in this study cannot be deposited in a public repository because the data could be potentially traced back to a single embryo and the donor. To request access, contact the corresponding author and the Stockholm Medical Biobank. It may be required to establish a Personal Data processing (PDP) Agreement and/or Data Transfer Agreement (DTA) according to General Data Protection Regulation (GDPR). Processed sequencing data is available from the Gene Expression Omnibus (GEO) under Superseries GSE220027 (subseries GSE220023, 220024, 220025 and 220026). All previously published datasets used in this study for untreated Day 0, 7, 13 and 20 are found in GEO GSE192858 (Subseries GSE192854, GSE192855, GSE192856, GSE192857).

The single-cell data can be explored in webtools for scRNA-seq (**hescneuroparacet**) and integrative scATAC-seq/scRNA-seq (**hescneurodiffparacet**) at https://cancell.medisin.uio.no/.
All code has been deposited in https://github.com/EskelandLab/Neuralparacet.

Table 3. Processed datasets are available in open access webtools.

Dataset	**Webtool**	**Hyperlink**
scRNA-seq	hescneuroparacet	https://cancell.medisin.uio.no/scrna/hescneuroparacet/
integrative scATAC-seq/scRNA-seq	hescneurodiffparacet	https://cancell.medisin.uio.no/scatac/hescneurodiffparacet/

List of abbreviations

ADHD: Attention Deficit/Hyperactivity Disorder
ATAC-seq: assay for transposase-accessible chromatin using sequencing
CREs: Cis Regulatory Elements
DEGs: differentially expressed genes
DMCs: differentially methylated CpGs
DMGs: differentially methylated genes
DNAm: DNA methylation
hESCs: human embryonic stem cells
NDDs: Neurodevelopmental disorders
RNA-seq: RNA sequencing
TF: Transcription factor
scATAC-seq: single-cell Assay for Transposase-Accessible Chromatin with sequencing
scRNA-seq: single-cell RNA sequencing
UMAP: Uniform Manifold approximation and projection

Declarations

Consent for publication. All authors have read and approved submission this version of the manuscript.

Competing interests
The authors declare that they have no competing interests.

Funding
We acknowledge funding from Research Council of Norway 262484 (R.E.), 241117 (R.L.), and 287953 (A.S.); the Swedish Research Council 2019-01157 (A.S.) and grants from the Swedish Brain FO2019-0087 (A.S.) and the Freemasons Children's House of Stockholm (A.S.) and BiomatDB+ (Horizon Europe #101058779; AS). We thank University of Oslo for open access publication support.

Authors' contributions

Conceptualization, M.S., A.S., R.E., K.G. and R.L.; Methodology, A.S., M.S., R.L., S.M., K.G., R.E., A.Sh., M.L., and M.F.; Writing – Original Draft, A.S., M.S., A.Sh., R.E., K.G. and R.L.; Writing – Review & Editing, A.S., M.S. R.L., K.G., R.E., A.Sh., M.L., H.N., and G.A.; Software, Formal Analysis, and Visualization, M.S., A.Sh., K.G., A.Y.M.S., R.L., and R.E.; Investigation and Validation, A.S., M.S., M.L., M.F., S.M., R.E. and K.G.; Funding, R.L., K.G., A.S., and R.E.; Supervision, R.L., K.G., H.N., A.S., and R.E.; Resources G.A., R.L., and R.E. All authors read and approved the final manuscript.

Acknowledgements

We thank Knut Waagan (University of Oslo) for technical assistance. The majority of informatic analysis was performed at Saga super computing resources (Project NN9632K) provided by UNINETT Sigma2—the National Infrastructure for High Performance Computing and Data Storage in Norway. The sequencing service was provided by the Norwegian Sequencing Centre (www.sequencing.uio.no), a national technology platform hosted by Oslo University Hospital and the University of Oslo and supported by the "Infrastructure" programs of the Research Council of Norway and the Southeastern Regional Health Authorities. PharmaTox Strategic Research Initiative was supported by Faculty of Mathematics and Natural Sciences, University of Oslo. We thank the The Norwegian Centre For Stem Cell Research for discussions at the initiation of this project. We would also like to thank Akshay Akshay (University of Bern) for his help in the fruitful discussion on single-cell ATAC-seq data analysis and visualization.

Authors' information (optional)

Ankush Sharma is now an employee of Acerta-Pharma, The Netherlands.

References

1. Lupattelli A, Spigset O, Twigg MJ, Zagorodnikova K, Mårdby AC, Moretti ME, et al. Medication use in pregnancy: A cross-sectional, multinational web-based study. BMJ Open. 2014 Feb 1;4(2):4365. Available from: http://bmjopen.bmj.com/
2. Zablotsky B, Black LI, Maenner MJ, Schieve LA, Danielson ML, Bitsko RH, et al. Prevalence and trends of developmental disabilities among children in the United States: 2009–2017. Pediatrics. 2019 Oct 1;144(4). Available from: www.aappublications.org/news
3. Werler MM, Mitchell AA, Hernandez-Diaz S, Honein MA. Use of over-the-counter medications during pregnancy. Am J Obstet Gynecol. 2005 Sep 1;193(3):771–7.
4. Nordeng H, Ystrøm E, Einarson A. Perception of risk regarding the use of medications and other exposures during pregnancy. Eur J Clin Pharmacol. 2010 Feb 20;66(2):207–14. Available from: https://link-springer-com.ezproxy.uio.no/article/10.1007/s00228-009-0744-2
5. Mcelhatton PR, Sullivan FM, Volans GN. Paracetamol overdose in pregnancy analysis of the outcomes of 300 cases referred to the Teratology Information Service. Reprod Toxicol. 1997;(I):85–94.
6. Liew Z, Ritz B, Rebordosa C, Lee P-C, Olsen J. Acetaminophen Use During Pregnancy, Behavioral Problems, and Hyperkinetic Disorders. JAMA Pediatr. 2014 Apr 1;168(4):313. Available from: http://www.ncbi.nlm.nih.gov/pubmed/24566677

7. Brandlistuen RE, Ystrom E, Nulman I, Koren G, Nordeng H. Prenatal paracetamol exposure and child neurodevelopment: a sibling-controlled cohort study. Int J Epidemiol. 2013 Dec 1;42(6):1702–13. Available from: http://www.ncbi.nlm.nih.gov/pubmed/24163279
8. Avella-Garcia CB, Julvez J, Fortuny J, Rebordosa C, García-Esteban R, Galán IR, et al. Acetaminophen use in pregnancy and neurodevelopment: attention function and autism spectrum symptoms. Int J Epidemiol. 2016 Jun 28;45(6):dyw115. Available from: https://academic.oup.com/ije/article-lookup/doi/10.1093/ije/dyw115
9. Stergiakouli E, Thapar A, Davey Smith G. Association of Acetaminophen Use During Pregnancy With Behavioral Problems in Childhood. JAMA Pediatr. 2016 Oct 1;170(10):964. Available from: http://archpedi.jamanetwork.com/article.aspx?doi=10.1001/jamapediatrics.2016.1775
10. Thompson JMD, Waldie KE, Wall CR, Murphy R, Mitchell EA, ABC study group. Associations between Acetaminophen Use during Pregnancy and ADHD Symptoms Measured at Ages 7 and 11 Years. Hashimoto K, editor. PLoS One. 2014 Sep 24;9(9):e108210. Available from: http://www.ncbi.nlm.nih.gov/pubmed/25251831
11. Bornehag C-G, Reichenberg A, Hallerback MU, Wikstrom S, Koch HM, Jonsson BA, et al. Prenatal exposure to acetaminophen and children's language development at 30 months. Eur Psychiatry. 2018 Jun 1;51:98–103. Available from: http://www.ncbi.nlm.nih.gov/pubmed/29331486
12. Ystrom E, Gustavson K, Brandlistuen RE, Knudsen GP, Magnus P, Susser E, et al. Prenatal exposure to acetaminophen and risk of ADHD. Pediatrics. 2017 Nov 1;140(5):20163840. Available from: www.aappublications.org/news
13. Trønnes JN, Wood M, Lupattelli A, Ystrom E, Nordeng H. Prenatal paracetamol exposure and neurodevelopmental outcomes in preschool□aged children. Paediatr Perinat Epidemiol. 2020 May 25;34(3):247–56. Available from: https://onlinelibrary.wiley.com/doi/abs/10.1111/ppe.12568
14. Sznajder KK, Teti DM, Kjerulff KH. Maternal use of acetaminophen during pregnancy and neurobehavioral problems in offspring at 3 years: A prospective cohort study. PLoS One 2022 Sep 28;17(9):e0272593. Available from: https://journals.plos.org/plosone/article?id=10.1371/journal.pone.0272593
15. Khan FY, Kabiraj G, Ahmed MA, Adam M, Mannuru SP, Ramesh V, et al. A Systematic Review of the Link Between Autism Spectrum Disorder and Acetaminophen: A Mystery to Resolve. Cureus 2022 Jul 19;14(7). Available from: /pmc/articles/PMC9385573/
16. European Medicines Agency (EMA), Pharmacovigilance Risk Assessment Committee (PRAC). PRAC recommendations on signals 2019. Available from: https://www.ema.europa.eu/en/documents/prac-recommendation/prac-recommendations-signals-adopted-12-15-march-2019-prac-meeting_en.pdf
17. Bauer AZ, Swan SH, Kriebel D, Liew Z, Taylor HS, Bornehag CG, et al. Paracetamol use during pregnancy — a call for precautionary action. Nat Rev Endocrinol 2021 1712. 2021 Sep 23;17(12):757–66. Available from: https://www-nature-com.ezproxy.uio.no/articles/s41574-021-00553-7
18. The European Network of Teratology Information Services (ENTIS). Position statement on acetaminophen (paracetamol) in pregnancy. 2021 Available from: https://www.entis-org.eu/wp-content/uploads/2021/10/ENTIS-position-statement-on-acetaminophen-3.10.2021.pdf
19. Gervin K, Nordeng H, Ystrom E, Reichborn-Kjennerud T, Lyle R. Long-term prenatal exposure to paracetamol is associated with DNA methylation differences in children diagnosed with ADHD. Clin Epigenetics. 2017 Dec 2;9(1):77. Available from:

http://clinicalepigeneticsjournal.biomedcentral.com/articles/10.1186/s13148-017-0376-9
20. Fragou D, Pakkidi E, Aschner M, Samanidou V, Kovatsi L. Smoking and DNA methylation: Correlation of methylation with smoking behavior and association with diseases and fetus development following prenatal exposure. 2019 ; Available from: https://doi.org/10.1016/j.fct.2019.04.059
21. Cornelius MD, De Genna NM, Leech SL, Willford JA, Goldschmidt L, Day NL. Effects of prenatal cigarette smoke exposure on neurobehavioral outcomes in 10-year-old children of adolescent mothers. Neurotoxicol Teratol. 2011 Jan;33(1):137–44. Available from: /pmc/articles/PMC3058878/
22. Tran NQV, Miyake K. Neurodevelopmental Disorders and Environmental Toxicants: Epigenetics as an Underlying Mechanism. Vol. 2017, International Journal of Genomics. Hindawi Limited; 2017.
23. Samara A, Falck M, Spildrejorde M, Leithaug M, Acharya G, Lyle R, et al. Robust neuronal differentiation of human embryonic stem cells for neurotoxicology. STAR Protoc. 2022;3:101533. Available from: https://doi.org/10.1016/j.xpro.2022.101533
24. Graham GG, Davies MJ, Day RO, Mohamudally A, Scott KF. The modern pharmacology of paracetamol: Therapeutic actions, mechanism of action, metabolism, toxicity and recent pharmacological findings. Vol. 21, Inflammopharmacology. Springer; 2013. p. 201–32. Available from: https://link-springer-com.ezproxy.uio.no/article/10.1007/s10787-013-0172-x
25. Trettin A, Böhmer A, Suchy MT, Probst I, Staerk U, Stichtenoth DO, et al. Effects of paracetamol on NOS, COX, and CYP activity and on oxidative stress in healthy male subjects, rat hepatocytes, and recombinant NOS. Oxid Med Cell Longev. 2014;2014.
26. Raffa RB, Pawasauskas J, Pergolizzi J V., Lu L, Chen Y, Wu S, et al. Pharmacokinetics of Oral and Intravenous Paracetamol (Acetaminophen) When Co-Administered with Intravenous Morphine in Healthy Adult Subjects. Clin Drug Investig. 2018 Mar 1;38(3):259–68. Available from: /pmc/articles/PMC5834589/
27. Samara A, Spildrejorde M, Sharma A, Gervin K, Lyle R, Eskeland R. A multi-omics approach to visualize early neuronal differentiation from hESCs in 4D. iScience. 2022; Available from: https://doi.org/10.1016/j.isci.
28. Baizabal JM, Mistry M, García MT, Gómez N, Olukoya O, Tran D, et al. The Epigenetic State of PRDM16-Regulated Enhancers in Radial Glia Controls Cortical Neuron Position. Neuron. 2018 Jun 6;98(5):945-962.e8.
29. Simões-Costa M, Bronner ME. Establishing neural crest identity: a gene regulatory recipe. Development. 2015 Jan 1;142(2):242. Available from: /pmc/articles/PMC4302844/
30. Pensold D, Zimmer G. Single-Cell Transcriptomics Reveals Regulators of Neuronal Migration and Maturation During Brain Development. J Exp Neurosci. 2018 Mar 6 12. Available from: /pmc/articles/PMC5846933/
31. Guo H, Duyzend MH, Coe BP, Baker C, Hoekzema K, Gerdts J, et al. Genome sequencing identifies multiple deleterious variants in autism patients with more severe phenotypes. Genet Med. 2019 Jul 1;21(7):1611. Available from: /pmc/articles/PMC6546556/
32. Chen J, Yen A, Florian CP, Dougherty JD. MYT1L in the making: emerging insights on functions of a neurodevelopmental disorder gene. Transl Psychiatry. 2022 Dec 1;12(1). Available from: /pmc/articles/PMC9307810/
33. Roesler MK, Lombino FL, Freitag S, Schweizer M, Hermans-Borgmeyer I, Schwarz JR, et al. Myosin XVI Regulates Actin Cytoskeleton Dynamics in Dendritic Spines of Purkinje Cells and Affects Presynaptic Organization. Front Cell Neurosci. 2019 Aug

13;13. Available from: /pmc/articles/PMC6705222/
34. Maïza A, Sidahmed-Adrar N, Michel PP, Carpentier G, Habert D, Dalle C, et al. 3-O-sulfated heparan sulfate interactors target synaptic adhesion molecules from neonatal mouse brain and inhibit neural activity and synaptogenesis in vitro. Sci Rep. 2020 Dec 1;10(1). Available from: /pmc/articles/PMC7644699/
35. Zhang Y, Li Y, Fan Y, Zhang X, Tang Z, Qi J, et al. SorCS3 promotes the internalization of p75NTR to inhibit GBM progression. Cell Death Dis. 2022 Apr 1;13(4). Available from: /pmc/articles/PMC8989992/
36. Tu L, Fukuda M, Tong Q, Xu Y. The ventromedial hypothalamic nucleus: watchdog of whole-body glucose homeostasis. Cell Biosci. 2022 Dec 1;12(1). Available from: /pmc/articles/PMC9134642/
37. Yap CC, Digilio L, McMahon L, Winckler B. The endosomal neuronal proteins Nsg1/NEEP21 and Nsg2/P19 are itinerant, not resident proteins of dendritic endosomes. Sci Rep. 2017 Dec 1;7(1). Available from: /pmc/articles/PMC5585371/
38. Tábara LC, Al-Salmi F, Maroofian R, Al-Futaisi AM, Al-Murshedi F, Kennedy J, et al. TMEM63C mutations cause mitochondrial morphology defects and underliehereditary spastic paraplegia. Brain. 2022 Sep 14;145(9):3095. Available from: /pmc/articles/PMC9473353/
39. Omotade OF, Rui Y, Lei W, Yu K, Hartzell HC, Fowler VM, et al. Tropomodulin Isoform-Specific Regulation of Dendrite Development and Synapse Formation. J Neurosci. 2018 Nov 11;38(48):10271. Available from: /pmc/articles/PMC6262146/
40. Bräuer AU, Savaskan NE, Kühn H, Prehn S, Ninnemann O, Nitsch R. A new phospholipid phosphatase, PRG-1, is involved in axon growth and regenerative sprouting. Nat Neurosci 2003 66. 2003 May 5;6(6):572–8. Available from: https://www.nature.com/articles/nn1052
41. Yu QS, Feng WQ, Shi LL, Niu RZ, Liu J. Integrated Analysis of Cortex Single-Cell Transcriptome and Serum Proteome Reveals the Novel Biomarkers in Alzheimer's Disease. Brain Sci. 2022 Aug 1;12(8). Available from: /pmc/articles/PMC9405865/
42. Zito A, Cartelli D, Cappelletti G, Cariboni A, Andrews W, Parnavelas J, et al. Neuritin 1 promotes neuronal migration. Brain Struct Funct. 2014 Jan 5;219(1):105–18. Available from: https://link-springer-com.ezproxy.uio.no/article/10.1007/s00429-012-0487-1
43. Wanigasekara Y, Airaksinen MS, Heuckeroth RO, Milbrandt J, Keast JR. Neurturin signalling via GFRα2 is essential for innervation of glandular but not muscle targets of sacral parasympathetic ganglion neurons. Mol Cell Neurosci. 2004 Feb 1;25(2):288–300.
44. Kessi M, Chen B, Peng J, Yan F, Yang L, Yin F. Calcium channelopathies and intellectual disability: a systematic review. Orphanet J Rare Dis. 2021 Dec 1;16(1). Available from: /pmc/articles/PMC8120735/
45. Smith RS, Kenny CJ, Ganesh V, Jang A, Borges-Monroy R, Partlow JN, et al. Sodium Channel SCN3A (NaV1.3) Regulation of Human Cerebral Cortical Folding and Oral Motor Development. Neuron. 2018 Sep 5;99(5):905-913.e7.
46. La Manno G, Gyllborg D, Codeluppi S, Nishimura K, Salto C, Zeisel A, et al. Molecular Diversity of Midbrain Development in Mouse, Human, and Stem Cells. Cell. 2016 Oct 6;167(2):566-580.e19.
47. Hou PS, hAilín D, Vogel T, Hanashima C. Transcription and Beyond: Delineating FOXG1 Function in Cortical Development and Disorders. Front Cell Neurosci. 2020 Feb 25;14. Available from: /pmc/articles/PMC7052011/
48. Méndez-Maldonado K, Vega-López GA, Aybar MJ, Velasco I. Neurogenesis From Neural Crest Cells: Molecular Mechanisms in the Formation of Cranial Nerves and

Ganglia. Front Cell Dev Biol. 2020 Aug 7;8. Available from: /pmc/articles/PMC7427511/
49. Zhang ZH, Song GL. Roles of Selenoproteins in Brain Function and the Potential Mechanism of Selenium in Alzheimer's Disease. Front Neurosci. 2021 Mar 8;15. Available from: /pmc/articles/PMC7982578/
50. Aiken J, Buscaglia G, Bates EA, Moore JK. The α-Tubulin gene TUBA1A in Brain Development: A Key Ingredient in the Neuronal Isotype Blend. J Dev Biol. 2017 Sep 1;5(3). Available from: /pmc/articles/PMC5648057/
51. Leandro-García LJ, Leskelä S, Landa I, Montero-Conde C, López-Jiménez E, Letón R, et al. Tumoral and tissue-specific expression of the major human β-tubulin isotypes. Cytoskeleton. 2010 Apr 1;67(4):214–23. Available from: https://onlinelibrary.wiley.com/doi/full/10.1002/cm.20436
52. Zhao Z, Zhang D, Yang F, Xu M, Zhao S, Pan T, et al. Evolutionarily conservative and non-conservative regulatory networks during primate interneuron development revealed by single-cell RNA and ATAC sequencing. Cell Res. 2022 May 1;32(5):425. Available from: /pmc/articles/PMC9061815/
53. Granja JM, Ryan Corces M, Pierce SE, Tansu Bagdatli S, Choudhry H, Chang HY, et al. ArchR is a scalable software package for integrative single-cell chromatin accessibility analysis.; Available from: https://doi.org/10.1038/s41588-021-00790-6
54. Ogryzko V V., Schiltz RL, Russanova V, Howard BH, Nakatani Y. The transcriptional coactivators p300 and CBP are histone acetyltransferases. Cell. 1996 Nov 29;87(5):953–9. Available from: http://www.cell.com.ezproxy.uio.no/article/S0092867400820012/fulltext
55. Lan F, Bayliss PE, Rinn JL, Whetstine JR, Wang JK, Chen S, et al. A histone H3 lysine 27 demethylase regulates animal posterior development. Nat 2007 4497163. 2007 Sep 12;449(7163):689–94. Available from: https://www.nature.com/articles/nature06192
56. Adra CN, Donato JL, Badovinac R, Syed F, Kheraj R, Cai H, et al. SMARCAD1, a Novel Human Helicase Family-Defining Member Associated with Genetic Instability: Cloning, Expression, and Mapping to 4q22–q23, a Band Rich in Breakpoints and Deletion Mutants Involved in Several Human Diseases. Genomics. 2000 Oct 15;69(2):162–73.
57. Mao Y, Lee AWM. A novel role for Gab2 in bFGF-mediated cell survival during retinoic acid–induced neuronal differentiation. J Cell Biol. 2005 Jul 7;170(2):305. Available from: /pmc/articles/PMC2171408/
58. Louvi A, Artavanis-Tsakonas S. Notch signalling in vertebrate neural development. Nat Rev Neurosci 2006 72. 2006 Feb;7(2):93–102. Available from: https://www.nature.com/articles/nrn1847
59. Holtz AM, Peterson KA, Nishi Y, Morin S, Song JY, Charron F, et al. Essential role for ligand-dependent feedback antagonism of vertebrate hedgehog signaling by PTCH1, PTCH2 AND HHIP1 during neural patterning. Dev. 2013 Aug 15;140(16):3423–34. Available from: /pmc/articles/PMC3737722/
60. Onishi K, Zou Y. Sonic Hedgehog switches on Wnt/planar cell polarity signaling in commissural axon growth cones by reducing levels of Shisa2. Elife. 2017 Sep 8;6. Available from: /pmc/articles/PMC5779225/
61. Sanders SS, Hernandez LM, Soh H, Karnam S, Walikonis RS, Tzingounis A V., et al. The palmitoyl acyltransferase ZDHHC14 controls Kv1-family potassium channel clustering at the axon initial segment. Elife. 2020 Oct 1;9:1–32. Available from: /pmc/articles/PMC7685708/
62. Imaizumi K, Tsuda M, Wanaka A, Tohyama M, Takagi T. Differential expression of sgk mRNA, a member of the Ser/Thr protein kinase gene family, in rat brain after CNS

injury. Mol Brain Res. 1994 Oct 1;26(1–2):189–96.
63. Pietzsch A, Büchler C, Schmitz G. Genomic Organization, Promoter Cloning, and Chromosomal Localization of the Dif-2 Gene. Biochem Biophys Res Commun. 1998 Apr 28;245(3):651–7.
64. Lim FT, Ogawa S, Parhar IS. Spred-2 expression is associated with neural repair of injured adult zebrafish brain. J Chem Neuroanat. 2016 Nov 1;77:176–86.
65. Yosten GLC, Harada CM, Haddock C, Giancotti LA, Kolar GR, Patel R, et al. GPR160 de-orphanization reveals critical roles in neuropathic pain in rodents. J Clin Invest. 2020 Apr 4;130(5):2587. Available from: /pmc/articles/PMC7190928/
66. Bennett KM, Liu J, Hoelting C, Stoll J. Expression and analysis of two novel rat organic cation transporter homologs, SLC22A17 and SLC22A23. Mol Cell Biochem. 2011 Jun;352(1–2):143. Available from: /pmc/articles/PMC3097276/
67. Kaiser A, Broeder C, Cohen JR, Douw L, Reneman L, Schrantee A. Effects of a single□dose methylphenidate challenge on resting□state functional connectivity in stimulant□treatment naive children and adults with ADHD. Hum Brain Mapp. 2022 Oct 10;43(15):4664. Available from: /pmc/articles/PMC9491277/
68. Grimm O, Thomä L, Kranz TM, Reif A. Is genetic risk of ADHD mediated via dopaminergic mechanism? A study of functional connectivity in ADHD and pharmacologically challenged healthy volunteers with a genetic risk profile. Transl Psychiatry. 2022 Dec 1;12(1). Available from: /pmc/articles/PMC9243079/
69. El Amine F, Heidinger B, Cameron JD, Hafizi K, Banifatemi S, Robaey P, et al. Two-month administration of methylphenidate improves olfactory sensitivity and suppresses appetite in individuals with obesity. Can J Physiol Pharmacol. 2022;100(5):432–40. Available from: https://cdnsciencepub-com.ezproxy.uio.no/doi/10.1139/cjpp-2021-0318
70. Yuan D, Zhang M, Huang Y, Wang X, Jiao J, Huang Y. Noradrenergic genes polymorphisms and response to methylphenidate in children with ADHD: A systematic review and meta-analysis. Medicine (Baltimore). 2021 Nov 11;100(46):e27858. Available from: /pmc/articles/PMC8601359/
71. Demontis D, Walters RK, Martin J, Mattheisen M, Als TD, Agerbo E, et al. Discovery of the first genome-wide significant risk loci for attention deficit/hyperactivity disorder. Nat Genet. 2019 Jan 1;51(1):63–75.
72. Sekaninova N, Mestanik M, Mestanikova A, Hamrakova A, Tonhajzerova I. Novel Approach to Evaluate Central Autonomic Regulation in Attention Deficit/Hyperactivity Disorder (ADHD). 2019; Available from: www.biomed.cas.cz/physiolresPhysiol.Res.68:531-545,2019https://doi.org/10.33549/physiolres.934160
73. Morris SSJ, Musser ED, Tenenbaum RB, Ward AR, Martinez J, Raiker JS, et al. Emotion Regulation via the Autonomic Nervous System in Children with Attention-Deficit/Hyperactivity Disorder (ADHD): Replication and Extension. J Abnorm Child Psychol. 2020 Mar 1;48(3):361. Available from: /pmc/articles/PMC7720673/
74. Griffiths KR, Quintana DS, Hermens DF, Spooner C, Tsang TW, Clarke S, et al. Sustained attention and heart rate variability in children and adolescents with ADHD. Biol Psychol. 2017;124:11–20. Available from: http://dx.doi.org/10.1016/j.biopsycho.2017.01.004
75. Montalbán-Loro R, Lassi G, Lozano-Ureña A, Perez-Villalba A, Jiménez-Villalba E, Charalambous M, et al. Dlk1 dosage regulates hippocampal neurogenesis and cognition. Proc Natl Acad Sci U S A. 2021 Mar 3;118(11). Available from: /pmc/articles/PMC7980393/
76. Tang J, Yu Y, Yang W. Long noncoding RNA and its contribution to autism spectrum

disorders. CNS Neurosci Ther. 2017 Aug 1;23(8):645. Available from: /pmc/articles/PMC6492731/
77. Zayats T, Johansson S, Haavik J. Expanding the toolbox of ADHD genetics. How can we make sense of parent of origin effects in ADHD and related behavioral phenotypes? Behav Brain Funct. 2015 Oct 16;11(1):33. Available from: /pmc/articles/PMC4609130/
78. Shimada IS, Acar M, Burgess RJ, Zhao Z, Morrison SJ. Prdm16 is required for the maintenance of neural stem cells in the postnatal forebrain and their differentiation into ependymal cells. Genes Dev. 2017 Jun 6;31(11):1134–46. Available from: /pmc/articles/PMC5538436/
79. Creyghton MP, Cheng AW, Welstead GG, Kooistra T, Carey BW, Steine EJ, et al. Histone H3K27ac separates active from poised enhancers and predicts developmental state. Proc Natl Acad Sci U S A. 2010 Dec 14;107(50):21931–6. Available from: https://www-pnas-org.ezproxy.uio.no/doi/abs/10.1073/pnas.1016071107
80. Bjørk MH, Zoega H, Leinonen MK, Cohen JM, Dreier JW, Furu K, et al. Association of Prenatal Exposure to Antiseizure Medication With Risk of Autism and Intellectual Disability. JAMA Neurol. 2022 Jul 1;79(7):672–81. Available from: https://jamanetwork-com.ezproxy.uio.no/journals/jamaneurology/fullarticle/2793003
81. Goasdoué K, Miller SM, Colditz PB, Björkman ST. Review: The blood-brain barrier; protecting the developing fetal brain. Placenta. 2017 Jun 1;54:111–6.
82. Eslamimehr S, Jones AD, Anthony TM, Arshad SH, Holloway JW, Ewart S, et al. Association of prenatal acetaminophen use and acetaminophen metabolites with DNA methylation of newborns: analysis of two consecutive generations of the Isle of Wight birth cohort. Environ Epigenetics. 2022;8(1):1–10. Available from: /pmc/articles/PMC8933617/
83. Olstad EW, Nordeng HME, Gervin K. Prenatal medication exposure and epigenetic outcomes: a systematic literature review and recommendations for prenatal pharmacoepigenetic studies. Epigenetics. 2021 Apr 29;1–24. Available from: https://www.tandfonline.com/doi/full/10.1080/15592294.2021.1903376
84. Addo KA, Bulka C, Dhingra R, Santos HP, Smeester L, O'Shea TM, et al. Acetaminophen use during pregnancy and DNA methylation in the placenta of the extremely low gestational age newborn (ELGAN) cohort. Environ Epigenetics. 2019 Apr 1;5(2):1–10. Available from: https://academic.oup.com/eep/article/5/2/dvz010/5544049
85. Ström S, Holm F, Bergström R, Strömberg AM, Hovatta O. Derivation of 30 human embryonic stem cell lines—improving the quality. In Vitro Cell Dev Biol Anim. 2010 Apr;46(3):337. Available from: /pmc/articles/PMC2855803/
86. Ávila-González D, Portillo W, García-López G, Molina-Hernández A, Díaz-Martínez NE, Díaz NF. Unraveling the Spatiotemporal Human Pluripotency in Embryonic Development. Front Cell Dev Biol. 2021 Jun 23;9. Available from: /pmc/articles/PMC8262797/
87. Ahokas RA, McKinney ET. Development and Physiology of the Placenta and Membranes. The Global Library of Women's Medicine. Sapiens Publishing, LTD; 2009. Available from: http://www.glowm.com/section-view/heading/Development and Physiology of the Placenta and Membranes/item/101
88. Conings S, Tseke F, Van Den Broeck A, Qi B, Paulus J, Amant F, et al. Transplacental transport of paracetamol and its phase II metabolites using the ex vivo placenta perfusion model. 2019; Available from: https://doi.org/10.1016/j.taap.2019.03.004
89. Cortes D, Pera MF. The genetic basis of inter-individual variation in recovery from traumatic brain injury. npj Regen Med 2021 61. 2021 Jan 21;6(1):1–9. Available from:

https://www-nature-com.ezproxy.uio.no/articles/s41536-020-00114-y
90. Finno CJ, Chen Y, Park S, Lee JH, Perez-Flores MC, Choi J, et al. Cisplatin Neurotoxicity Targets Specific Subpopulations and K+ Channels in Tyrosine-Hydroxylase Positive Dorsal Root Ganglia Neurons. Front Cell Neurosci. 2022 May 2;16. Available from: /pmc/articles/PMC9108181/
91. Jayanthi S, Daiwile AP, Cadet JL. Neurotoxicity of methamphetamine: main effects and mechanisms. Exp Neurol. 2021 Oct 1;344:113795. Available from: /pmc/articles/PMC8338805/
92. Thapa D, Wu K, Stoner MW, Xie B, Zhang M, Manning JR, et al. The protein acetylase GCN5L1 modulates hepatic fatty acid oxidation activity via acetylation of the mitochondrial β-oxidation enzyme HADHA. J Biol Chem. 2018 Nov 11;293(46):17676. Available from: /pmc/articles/PMC6240879/
93. Schroeder BC, Waldegger S, Fehr S, Bleich M, Warth R, Greger R, et al. A constitutively open potassium channel formed by KCNQ1 and KCNE3. Nat 2000 4036766. 2000 Jan 13;403(6766):196–9. Available from: https://www.nature.com/articles/35003200
94. Miura R, Araki A, Minatoya M, Miyake K, Chen ML, Kobayashi S, et al. An epigenome-wide analysis of cord blood DNA methylation reveals sex-specific effect of exposure to bisphenol A. Sci Rep. 2019 Dec 1;9(1):1–13. Available from: https://doi.org/10.1038/s41598-019-48916-5
95. Koehn LM, Huang Y, Habgood MD, Nie S, Chiou SY, Banati RB, et al. Efflux transporters in rat placenta and developing brain: transcriptomic and functional response to paracetamol. Sci Rep. 2021 Dec 1;11(1). Available from: /pmc/articles/PMC8494792/
96. Koenderink JB, van den Heuvel JJMW, Bilos A, Vredenburg G, Vermeulen NPE, Russel FGM. Human multidrug resistance protein 4 (MRP4) is a cellular efflux transporter for paracetamol glutathione and cysteine conjugates. Arch Toxicol 2020 Sep 1;94(9):3027. Available from: /pmc/articles/PMC7415487/
97. Koehn LM, Huang Y, Habgood MD, Kysenius K, Crouch PJ, Dziegielewska KM, et al. Effects of paracetamol (acetaminophen) on gene expression and permeability properties of the rat placenta and fetal brain. F1000Research. 2020;9. Available from: /pmc/articles/PMC7477648/
98. Mahley RW, Huang Y. Apolipoprotein E Sets the Stage: Response to Injury Triggers Neuropathology, Including Alzheimer's Disease. Neuron. 2012 Dec 12;76(5):871. Available from: /pmc/articles/PMC4891195/
99. Malik AR, Willnow TE. Excitatory Amino Acid Transporters in Physiology and Disorders of the Central Nervous System. Int J Mol Sci. 2019 Nov 2;20(22). Available from: /pmc/articles/PMC6888459/
100. Tüshaus J, Müller SA, Kataka ES, Zaucha J, Monasor LS, Su M, et al. An optimized quantitative proteomics method establishes the cell type resolved mouse brain secretome. EMBO J. 2020 Oct 10;39(20). Available from: /pmc/articles/PMC7560198/
101. Ouyang JF, Kamaraj US, Cao EY, Rackham OJL. ShinyCell: simple and sharable visualization of single-cell gene expression data. Bioinformatics. 2021 Oct 11;37(19):3374–6. Available from: https://academic.oup.com/bioinformatics/article/37/19/3374/6198103
102. Sharma A, Akshay A, Rogne M, Eskeland R. ShinyArchR.UiO: user-friendly,integrative and open-source tool for visualization of single-cell ATAC-seq data using ArchR. Bioinformatics. 2022 Jan 12;38(3):834–6. Available from: https://academic.oup.com/bioinformatics/article/38/3/834/6377776
103. Main H, Hedenskog M, Acharya G, Hovatta O, Lanner F. Karolinska Institutet Human

Embryonic Stem Cell Bank. Stem Cell Res. 2020 May 1;45:101810.
104. Nitsche J, Patil A, Langman L, Penn H, Derleth D, Watson W, et al. Transplacental Passage of Acetaminophen in Term Pregnancy. Am J Perinatol. 2017 Nov 2;34(06):541–3. Available from: http://www.thieme-connect.de/DOI/DOI?10.1055/s-0036-1593845
105. Bannwarth B, Netter P, Lapicque F, Gillet P, Pere P, Boccard E, et al. Plasma and cerebrospinal fluid concentrations of paracetamol after a single intravenous dose of propacetamol. Br J Clin Pharmacol. 1992;34(1):79. Available from: /pmc/articles/PMC1381380/?report=abstract
106. Anderson BJ, Holford NHG, Woollard GA, Chan PLS. Paracetamol plasma and cerebrospinal fluid pharmacokinetics in children. Br J Clin Pharmacol. 1998;46(3):237–43. Available from: /pmc/articles/PMC1873683/
107. Kumpulainen E, Kokki H, Halonen T, Heikkinen M, Savolainen J, Laisalmi M. Paracetamol (acetaminophen) penetrates readily into the cerebrospinal fluid of children after intravenous administration. Pediatrics. 2007 Apr 1 [;119(4):766–71. Available from: www.pediatrics.org/cgi/doi/10.1542/
108. Coulter SJ. Mitigation of the effect of variability in digital PCR assays through use of duplexed reference assays for normalization. Biotechniques. 2018 Aug 9;65(2):86–91. Available from: https://www.future-science.com/doi/10.2144/btn-2018-0058
109. Kassambara A. ggpubr: “ggplot2” Based Publication Ready Plots. 2020.
110. Wickham H, Averick M, Bryan J, Chang W, McGowan L, François R, et al. Welcome to the Tidyverse. J Open Source Softw. 2019 Nov 21;4(43):1686. Available from: https://joss.theoj.org/papers/10.21105/joss.01686
111. Bushnell B. BBMap: A Fast, Accurate, Splice-Aware Aligner. United States; 2014. Available from: https://www.osti.gov/biblio/1241166
112. Kim D, Langmead B, Salzberg SL. HISAT: A fast spliced aligner with low memory requirements. Nat Methods. 2015 Mar 31;12(4):357–60. Available from: /pmc/articles/PMC4655817/?report=abstract
113. Liao Y, Smyth GK, Shi W. FeatureCounts: An efficient general purpose program for assigning sequence reads to genomic features. Bioinformatics. 2014 Apr 1;30(7):923–30. Available from: https://pubmed.ncbi.nlm.nih.gov/24227677/
114. R Core Team. R: A language and environment for statistical computing. Vienna, Austria: R Foundation for Statistical Computing; 2021. Available from: https://www.r-project.org/
115. Varet H, Brillet-Guéguen L, Coppée JY, Dillies MA. SARTools: A DESeq2- and EdgeR-Based R Pipeline for Comprehensive Differential Analysis of RNA-Seq Data. PLoS One. 2016 Jun 1;11(6):e0157022. Available from: https://journals.plos.org/plosone/article?id=10.1371/journal.pone.0157022
116. Love MI, Huber W, Anders S. Moderated estimation of fold change and dispersion for RNA-seq data with DESeq2. Genome Biol. 2014 Dec 5;15(12):550. Available from: http://genomebiology.biomedcentral.com/articles/10.1186/s13059-014-0550-8
117. Kolde R. pheatmap: Pretty Heatmaps. 2019.
118. Subramanian A, Tamayo P, Mootha VK, Mukherjee S, Ebert BL, Gillette MA, et al. Gene set enrichment analysis: A knowledge-based approach for interpreting genome-wide expression profiles. Proc Natl Acad Sci U S A. 2005 Oct 25;102(43):15545–50. Available from: www.pnas.orgcgidoi10.1073pnas.0506580102
119. Aryee MJ, Jaffe AE, Corrada-Bravo H, Ladd-Acosta C, Feinberg AP, Hansen KD, et al. Minfi: A flexible and comprehensive Bioconductor package for the analysis of Infinium DNA methylation microarrays. Bioinformatics. 2014 May 15;30(10):1363–9. Available from: /pmc/articles/PMC4016708/?report=abstract

120. Triche TJ, Weisenberger DJ, Van Den Berg D, Laird PW, Siegmund KD. Low-level processing of Illumina Infinium DNA Methylation BeadArrays. Nucleic Acids Res. 2013 Apr;41(7):e90. Available from: /pmc/articles/PMC3627582/?report=abstract
121. Fortin JP, Labbe A, Lemire M, Zanke BW, Hudson TJ, Fertig EJ, et al. Functional normalization of 450k methylation array data improves replication in large cancer studies. Genome Biol. 2014 Dec 3;15(11):503. Available from: http://genomebiology.biomedcentral.com/articles/10.1186/s13059-014-0503-2
122. Ritchie ME, Phipson B, Wu D, Hu Y, Law CW, Shi W, et al. Limma powers differential expression analyses for RNA-sequencing and microarray studies. Nucleic Acids Res. 2015 Jan 6;43(7):e47. Available from: https://pubmed.ncbi.nlm.nih.gov/25605792/
123. Ren X, Kuan PF. methylGSA: a Bioconductor package and Shiny app for DNA methylation data length bias adjustment in gene set testing. 2019;
124. Stuart T, Butler A, Hoffman P, Hafemeister C, Papalexi E, Mauck WM, et al. Comprehensive Integration of Single-Cell Data. Cell. 2019 Jun 13;177(7):1888-1902.e21. Available from: http://www.cell.com.ezproxy.uio.no/article/S0092867419305598/fulltext
125. McCarthy DJ, Campbell KR, Lun ATL, Wills QF. Scater: pre-processing, quality control, normalization and visualization of single-cell RNA-seq data in R. Bioinformatics. 2017 Apr 4;33(8):1179. Available from: /pmc/articles/PMC5408845/
126. Hafemeister C, Satija R. Normalization and variance stabilization of single-cell RNA-seq data using regularized negative binomial regression. bioRxiv. 2019 Mar 14;576827. Available from: https://doi.org/10.1101/576827
127. Tirosh I, Izar B, Prakadan SM, Wadsworth MH, Treacy D, Trombetta JJ, et al. Dissecting the multicellular ecosystem of metastatic melanoma by single-cell RNA-seq. Science (80-). 2016 Apr 8;352(6282):189–96. Available from: http://science.sciencemag.org/
128. Zappia L, Oshlack A. Clustering trees: a visualization for evaluating clusterings at multiple resolutions. Gigascience 2018 Jul 1;7(7). Available from: /pmc/articles/PMC6057528/
129. Aran D, Looney AP, Liu L, Wu E, Fong V, Hsu A, et al. Reference-based analysis of lung single-cell sequencing reveals a transitional profibrotic macrophage. Nat Immunol 2019 202. 2019 Jan 14;20(2):163–72. Available from: https://www-nature-com.ezproxy.uio.no/articles/s41590-018-0276-y
130. Risso D, Cole M. scRNAseq: Collection of Public Single-Cell RNA-Seq Datasets. 2022. Available from: https://bioconductor.org/packages/release/data/experiment/html/scRNAseq.html